IL-12-expressing highly immunogenic recombinant modified vaccinia virus Ankara reprograms tumor-infiltrating myeloid cells to overcome immune resistance

Shuaitong Liu[1#], Gregory Mazo[1#], Ning Yang[1], Tuo Zhang[5], Yi Wang[1], Shanza Baseer Tariq[1], Yueqi Wang[1], Daniel Hirschhorn-Cymerman[9,10], Liangliang Ji[8], Adrian Tan[3], Jiahu Wang[6], Wei Yan[7], John Choi[7], Jenny Zhaoying Xiang[5], Ming O. Li[8], Taha Merghoub[2,3,4,9,10], Jedd D. Wolchok[2,4,9,10], and Liang Deng[1,9,10,11]*

[1]Dermatology Service, Department of Medicine, Memorial Sloan Kettering Cancer Center, New York, NY 10065, USA.

[2]Department of Medicine, Weill Cornell Medicine, New York, New York, USA.

[3]Department of Pharmacology, Weill Cornell Medicine, New York, New York, USA.

[4]Sandra and Edward Meyer Cancer Center, Weill Cornell Medicine, New York, New York, USA

[5]Genomic Resources Core Facility, Weill Cornell Medical College, New York, NY, 10065, USA

[6]Genvira Biosciences, Ottawa, ON K1V 1C1, Canada

[7]IMVAQ Therapeutics, Sammamish, WA, 98021, USA

[8]Immunology Program, Memorial Sloan Kettering Cancer Center

[9]Human Oncology and Pathogenesis Program; Memorial Sloan Kettering Cancer Center, New York, NY 10065, USA

[10]Parker Institute for Cancer Immunotherapy, Memorial Sloan Kettering Cancer Center, New York, NY, USA

[11]Department of Dermatology, Weill Cornell Medical College, New York, NY 10065

*corresponding author. Mailing address for Liang Deng: Dermatology Service, Department of Medicine, Memorial Sloan Kettering Cancer Center, 1275 York Ave., New York, NY 10065. Email: dengl@mskcc.org. [#] These two authors contributed equally to this work.

Abstract

Novel strategies to reprogram tumor-infiltrating myeloid cells for cancer immunotherapy are urgently needed, given that the primary and acquired resistance to immune checkpoint blockade (ICB) therapy has hindered the overall success of immunotherapy. Modified vaccinia virus Ankara (MVA) is a highly attenuated, non-replicative vaccinia virus and an approved vaccine against smallpox and monkeypox. Here we report rational engineering of recombinant MVA, MQ833, by removing three immune suppressive genes, E5R, E3L, and WR199, from the MVA genome and inserting three transgenes encoding Flt3L, OX40L, and IL-12. Intratumoral (IT) delivery of MQ833 generates potent antitumor responses dependent on $CD8^+$ T cells, neutrophils, and M1-like macrophages, the nucleic acid-sensing pathways mediated by MDA5/STING, and interferon feedback loop. IT MQ833 promotes the recruitment and activation of neutrophils and inflammatory monocytes into the injected tumors, depletion of M2-like macrophages, and expansion of M1-like macrophages, generating potent antitumor immunity against tumors resistant to ICB.

Introduction

The tumor immune microenvironment (TIME) comprises heterogeneous types of myeloid cells and lymphocytes, whose antitumor functions are often disabled by the hostile environment of growing tumors[1, 2, 3]. The major challenges of cancer immunotherapy are to reprogram myeloid cells and to reinvigorate lymphocytes for potent and persistent antitumor activities[4, 5, 6, 7, 8, 9]. Immunogenic viruses are one of the strategies to alter TIME for enhancing antitumor immunity[10, 11, 12, 13]. However, whether viral replication and oncolysis are required for viral-induced antitumor immunity is still being debated[14, 15, 16, 17].

Modified vaccinia virus Ankara (MVA) is a large cytoplasmic non-replicative DNA virus derived from replicating vaccinia virus Ankara strain through 570 passages in chicken embryonic fibroblasts leading to its attenuation[18]. The MVA genome contains large deletions and mutations in genes involved in virus-host interaction and viral immune evasion[19]. MVA was recently approved as a vaccine against smallpox and monkeypox[20], and has been investigated intensively as a vaccine vector against other infectious diseases and cancers[21,22]. The advantages of using MVA as a viral vector for cancer immunotherapy include: (i) its safety in the normal population and immune-compromised patients such as those with human immunodeficiency virus (HIV) infection[23]; (ii) its large DNA genome, which offers stability and space for transgene insertion; (iii) its ability to infect multiple cell types including tumor and immune cells and efficient expression of transgenes in the infected cells; and (iv) the immunogenicity of the virus, which can be further improved by removing immune suppressive genes.

We have previously shown that MVA infection of dendritic cells can moderately induce type I interferon production via the cytosolic DNA-sensing pathway dependent on cyclic GMP-AMP synthase (cGAS)[24]. Intratumoral injection of heat-inactivated MVA generates potent antitumor immunity via cGAS and is dependent on $CD8^+$ T cells and Batf3-dependent $CD103^+$ dendritic cells[17]. We also compared the antitumor immunity of live oncolytic vaccinia virus with a heat-inactivated version and found that inactivated oncolytic vaccinia generates more potent antitumor effects[16]. These results led us to conclude that vaccinia viral replication and oncolysis is not essential for the induction of antitumor immunity. Instead, the activation of the innate

47 immune system within the tumor is crucial for antitumor responses. Based on these results, we
48 engineered our first generation non-replicative recombinant MVA (rMVA or MQ710),
49 MVAΔE5R-Flt3L-OX40L, which activates the cGAS/STING pathway and depletes immune-
50 suppressive $OX40^{hi}$ regulatory T cells via OX40L-OX40 interaction and IFNAR signaling[25].
51 However, how innate immune sensing and type I IFN pathways contribute to viral-induced
52 antitumor immunity at individual immune cell type is not well understood.
53
54 In this study, we designed our second generation recombinant MVA (MQ833) by deleting two
55 more immune suppressive genes and adding a third transgene encoding an extracellular matrix-
56 anchored interleukin 12 (IL-12). Our results demonstrated that in addition to promoting the
57 generation of effector $CD8^+$ T cells, intratumoral (IT) delivery of IL-12 expressing immunogenic
58 recombinant MVA results in the recruitment and activation of neutrophils and M1-like
59 macrophages via the nucleic acid-sensing pathways and IFN signaling. As a result, IT MQ833
60 demonstrated antitumor efficacy in $B2m^{-/-}$ tumors resistant to $CD8^+$ T cell killing. Collectively,
61 our results provide novel insights into how IT IL-12 expressing immunogenic virus reprograms
62 myeloid cells for antitumor immunity.

63 **Results**

64

65 **The design of a highly immunogenic second-generation recombinant MVA (MQ833)**

66

67 Our previous study identified that the E5R gene of the MVA genome encodes a potent inhibitor
68 of the DNA sensor cGAS[26]. Infection of mouse bone marrow-derived dendritic cells (BMDCs)
69 with MVA lacking the E5R gene (MVAΔE5R) generates high levels of IFN-β production and
70 promotes DC maturation, which is dependent on cGAS[26]. We engineered our first-generation
71 recombinant MVA (rMVA or MQ710), MVAΔE5R-hFlt3L-mOX40L, by inserting an
72 expression cassette containing two transgenes encoding membrane-bound human Flt3L and
73 murine OX40L linked by a P2A self-cleaving sequence into the E5R gene[25]. Flt3L encodes a
74 growth factor for DCs[27], and OX40L encodes a co-stimulatory ligand for OX40-expressing T
75 cells[28]. Intratumoral (IT) delivery of rMVA (MQ710) generates strong antitumor immunity in
76 multiple tumor models, which is dependent on $CD8^+$ T cells, the cGAS/STING pathway, and
77 IFNAR feedback loop[25]. IT rMVA (MQ710) also leads to depletion of intratumoral $OX40^{hi}$
78 regulatory T cells via OX40L/OX40 interaction and IFNAR signaling[25]. To further potentiate the
79 antitumor efficacy of the virus, we designed our second-generation recombinant MVA (MQ833)
80 by removing two more viral immune evasion genes, E3L and WR199, and inserting the gene
81 encoding interleukin 12 (IL-12) anchored to extracellular matrix to prevent systemic toxicity.

82

83 **Vaccinia E3 and E5 synergize to inhibit the MDA5/STING-mediated nucleic acid-sensing**
84 **pathways in tumor cell lines**

85 Our previous work has shown that the vaccinia E3L gene encodes another viral immune evasion
86 factor that attenuates the cytosolic dsRNA sensing pathway[29]. Deleting both the E5R and E3L
87 genes in MVA synergistically boosted type I IFN production in multiple tumor cell lines
88 (Extended Data Fig. 1a). To assess whether this effect is dependent on the MDA5 and STING
89 signaling pathways, we generated *Mda5*$^{-/-}$ and *Mda5*$^{-/-}$*Sting*$^{-/-}$ B16-F10 cell lines using CRISPR-
90 Cas9. MVAΔE3LΔE5R infection resulted in elevated p-IRF-3 production in WT B16-F10 cells.
91 However, in *Mda5*$^{-/-}$ tumor cells, p-IRF-3 induction was dramatically reduced. MVAΔE3LΔE5R
92 failed to induce p-IRF-3 in *Mda5*$^{-/-}$*Sting*$^{-/-}$ B16 cells (Extended Data Fig. 1b). In addition,
93 MVAΔE3LΔE5R induced IFN-β secretion from B16-F10 cells was attenuated in *Mda5*$^{-/-}$ and

94 *Mda5*$^{-/-}$*Sting*$^{-/-}$ B16-F10 cells (Extended Data Fig. 1c). These results indicate that
95 MVAΔE3LΔE5R-induced IFN production in melanoma cells depends on MDA5 and STING-
96 mediated pathways.
97
98 **Deletion of the E3L gene from MQ710 improves the generation of tumor-specific T cells in**
99 **vivo**
100 We made sequential depletions in rMVA (MQ710) to generate rMVAΔE3L and
101 rMVAΔE3LΔWR199 (MQ832) and assessed the generation of antitumor T cells in vivo. In a
102 bilateral B16-F10 murine melanoma model, 5 x 10^5 and 2.5 x 10^5 B16-F10 cells were
103 intradermally implanted into the right and left flanks, respectively. When the tumors were
104 established, the larger tumors were injected twice three days apart with either heat-inactivated
105 MVA (Heat-iMVA), rMVA (MQ710), or rMVAΔE3L. PBS was used as a control (Extended
106 Data Fig. 2a). IT rMVA (MQ710) and rMVAΔE3L generated higher levels of Gzmb$^+$ CD8$^+$ T
107 cells in the injected and non-injected tumors compared with heat-iMVA or PBS (Extended Data
108 Fig. 2b). IT rMVA (MQ710) and rMVAΔE3L reduced OX40$^+$ Tregs in the injected tumors
109 whereas IT heat-iMVA failed to do so (Extended Data Fig. 2c). ELISPOT result showed that
110 rMVAΔE3L treatment generated stronger antitumor T cell responses in the spleens than rMVA
111 (MQ710) or Heat-iMVA (Extended Data Fig. 2d).
112
113 The vaccinia WR199, also known as the MVA186 gene, encodes a 68-kDa protein consisting of
114 N-terminal ankyrin repeats and a C-terminal F-box-like domain. WR199 protein interacts with
115 the SCF (Skp1, cullin1, F-box-containing complex) via the F-box-like domain[30] and is reported
116 to be involved in poxvirus genome uncoating and DNA replication in mammalian cells[31]. In
117 addition to E5, WR199 protein was also identified as a cGAS inhibitor[26], although its mechanism
118 of action is still under investigation. We generated rMVAΔE3LΔWR199 by deleting WR199
119 from rMVAΔE3L and named this virus as MQ832. IT MQ832 generated slightly higher levels of
120 Gzmb$^+$CD8$^+$ T cells and lower levels of OX40^{hi}Tregs than rMVAΔE3L (Extended Data Fig.
121 2e,f).
122
123 Interleukin 12 (IL-12) is a well-studied cytokine for its stimulatory effect on T and NK cells[32,33]
124 and local delivery of IL-12 expressed by oncolytic viruses enhanced antitumor potential [34,35,36].

125 IL-12 is a disulfide-linked heterodimer composed of p40 subunit encoded by the Il12b gene and
126 p35 subunit encoded by the Il12a gene. To further potentiate the immunogenicity of our virus,
127 we inserted an expression cassette with Il12b and Il12a linked by sequences encoding the P2A
128 peptides under the control of a modified H5 promoter [37] into the WR199 locus to generate the
129 final product MQ833 (Fig. 1a,b). In addition, the p35 subunit of Il-12 is tagged with matrix-
130 binding sequence at the C-terminus to prevent its systemic release and associated toxicities (Fig.
131 1a,b).
132
133 **MQ833 activates the cGAS/STING mediated DNA-sensing pathway and promotes IFN**
134 **production**
135
136 We first verified the expression of the three transgenes by flow cytometry and ELISA (Fig. 1c,
137 d). Infection of B16-F10 murine melanoma cells with MQ833 results in the robust expression of
138 hFlt3L and mOX40L on the surface of infected cells at 16 h post-infection (Fig. 1c). MQ833
139 infection of B16-F10 cells also resulted in the secretion of mIL-12 as determined by ELISA of
140 mIL-12p40 (Fig. 1d). Infection of MQ832 and MQ833 resulted in strong induction of *Ifnb* gene
141 expression and IFN-β production in B16-F10 cells (Fig. 1e, f). Western blot analyses showed
142 stronger induction of phosphorylation of STING and IRF3 in MQ832 and MQ833-infected B16-
143 F10 cells compared with MVA (Fig. 1g). These findings indicate that the triple deletion of E5R,
144 E3L, and WR199 caused dramatic enhancement of the ability of the virus to induce type I IFN
145 production and proinflammatory cytokines and chemokines from infected tumor cells in vitro. In
146 addition, Both MQ832 and MQ833 infection in BMDC led to high levels of IFN-β production in
147 a STING-dependent manner (Fig. 1h). MQ833 infection in BMDCs resulted in activation of the
148 cGAS/STING pathway and elevated p-IRF3 expression (Fig. 1i).
149
150 To test whether IL-12 expression by MQ833 promotes antigen-specific T cell activation, $CD11c^{+}$
151 splenic DCs isolated from WT or $cGAS^{-/-}$ mice were infected with MVA, MVAΔE5R, or
152 MQ833 at a MOI of 3. Cells were then pulsed with OVA and washed after three hours, and then
153 incubated with OT-1 cells at a DC:T cell ratio of 1:3. Supernatants were collected and IFN-γ
154 levels in the supernatants were determined by ELISA (Fig. 1j). MQ833 infection of DCs resulted
155 in much higher levels of IFN-γ production compared with MVAΔE5R (Fig. 1k). Whereas

156 MVAΔE5R-induced OT-1 T cell activation was largely dependent on cGAS, MQ833-induced
157 OT-1 cell activation was slightly reduced when co-cultured with cGAS$^{-/-}$ DCs (Fig. 1k). These
158 results demonstrated that the IL-12 in MQ833 is functional, and MQ833-induced antigen cross-
159 presentation is only partially dependent on cGAS. We also generated Flt3L-cultured BMDCs and
160 sorted CD103^{+} DCs for antigen cross-presentation assay. Similar to what we observed in splenic
161 CD11c DCs, infection of cultured CD103^{+} DCs with MQ833 promoted antigen cross-
162 presentation and antigen-specific T cell activation at a much higher level than MVAΔE5R (Fig.
163 1j,l). To test whether MQ833-induced T cell activation requires DC and T cell contact, we
164 collected supernatants from infected BMDCs and incubated them with OT-1 cells for three days.
165 Adding supernatants from BMDCs infected with MQ833 stimulated OT-1 T cells to produce
166 IFN-γ, but they produced much lower levels of IFN-γ without DCs compared with DC/T cell co-
167 culture (Fig. 1j,m).
168
169 **Validation of clinical candidate hMQ833 (MVAΔE5R-hFlt3L-hOX40L-ΔE3L-ΔWR199-**
170 **hIL-12)**
171 We engineered a humanized MQ833 (hMQ833) by substituting mOX40L and mIL-12 with their
172 human counterparts. Infection of human monocyte-derived DCs (moDCs) with hMQ833 resulted
173 in the expression of hFlt3L and hOX40L on the cell surface of infected cells (Extended Data Fig.
174 3a) at similar levels as hMQ710 (MVAΔE5R-hFlt3L-hOX40L). ELISA analysis of the
175 supernatants revealed high levels of IL-12p70 protein secreted by moDCs infected by hMQ833
176 but not by hMQ710 (Extended Data Fig. 3b). Infection of moDCs with hMQ833 resulted in
177 stronger induction of IFNB and CXCL10 gene expression than hMQ710 determined by RT-PCR
178 analysis (Extended Data Fig. 3c).
179
180 To test whether human IL-12 (hIL-12) produced by hMQ833-infected moDCs is functional, we
181 performed a co-culture experiment in which human moDCs were infected with either MVA,
182 hMQ710, mMQ833, or hMQ833 for 1 h, then cells were washed to remove the viruses and co-
183 cultured with either allogenic or autologous CD4 or CD8 T cells at a DC:T ratio of 1:5.
184 Supernatants were collected at 72 h post co-culture. IFN-γ levels in the supernatants were
185 measured by ELISA (Extended Data Fig. 3d). In the allogenic DC and T cell co-culture
186 conditions, hMQ833 infection of moDCs resulted higher levels of IFN-γ secretion by activated T

187 cells compared with mMQ833. Allogenic CD4 T cells secreted more IFN-γ than CD8 T cells.
188 Neither MVA nor hMQ710 promoted IFN-γ secretion. These results indicate that both hIL-12
189 produced by moDCs infected with hMQ833 and mIL-12 produced by moDCs infected with
190 mMQ833 were able to stimulate allogenic CD4 or CD8 T cells to produce IFN-γ, with the hIL-
191 12 being more potent than mIL-12.
192
193 In the autologous DC and T cell co-culture conditions, IFN-γ levels were lower than those
194 observed in the allogeneic DC and T cell co-culture, and autologous CD4 and CD8 T cells, once
195 stimulated by DCs, produced similar levels of IFN-γ. hIL-12 was more potent than mIL-12 in
196 stimulating autologous CD4 and CD8 T cells to produce IFN-γ (Extended Data Fig. 3e).
197
198 **Intratumoral delivery of MQ833 expressing IL-12 generates more potent antitumor effects**
199 **than MQ832**
200 Next, we compared the antitumor effects of MQ833 with MQ832 in a murine B16-F10
201 melanoma model. Briefly, B16-F10 murine melanoma cells were implanted intradermally in
202 C57BL/6J mice. MQ833 were injected into the tumors twice weekly (4 x 10^7 pfu per mouse per
203 injection) and tumor sizes were measured, and mouse survival was monitored (Fig. 2a).
204 Intratumoral delivery of MQ833 generates a 100% cure in B16-F10 tumor-bearing mice,
205 significantly higher than the 40% survival rate generated by MQ832 treatment (Fig. 2b-d). IT
206 MQ833 also resulted in 100% cure in a MC38 murine colon cancer model compared with 60%
207 cure in the group of mice treated with MQ832 (Extended Data Fig. 4a,b). These results indicate
208 that in a unilateral tumor model, IT MQ833 treatment resulted in better antitumor efficacy than
209 MQ832. In a large tumor bilateral MC38 tumor implantation model, we found that IT MQ833
210 was more effective than MQ832 in delaying tumor growth and extending medium survival time
211 (Extended Data Fig. 4c-e).
212
213 To test the abscopal antitumor response induced by IT MQ833 and whether that could be
214 enhanced with the combination of systemic delivery of ICB, we used a bilateral B16-F10
215 implantation model. Briefly, 7.5 x 10^5 and 1.5 x 10^5 B16-F10 were implanted intradermally into
216 the right and left flanks of C57BL/6J mice. MQ833 or MQ832 were injected into the tumors on
217 the right flank twice weekly. IT MQ833 eradicated most of injected tumors, significantly delayed

218 distal non-injected tumor growth and generated a 40% cure in this bilateral model, whereas
219 tumor-bearing mice treated IT MQ832 had no survivors (Extended Data Fig. 5a-c). Combination
220 therapy of IT MQ833 with intraperitoneal delivery of anti-PD1, anti-PD-L1, and anti-CTLA-4
221 antibodies resulted in a survival rate of 60% (Extended Data Fig. 5a-c). Collectively, these
222 results indicate that IT MQ833 generates stronger abscopal effects in the noninjected tumors than
223 MQ832, which can be synergized with systemic delivery of ICB.
224
225 We hypothesized that modulation of the tumor-infiltrating T cells might account for the MQ833-
226 induced antitumor efficacy. Using a bilateral B16-F10 tumor implantation model, we
227 intratumorally delivered MQ833 or MQ832 into the larger tumors on the right flanks twice with
228 three days apart. Both the injected and non-injected tumors were harvested two days after the
229 second injection. We observed that both MQ833 and MQ832 treatment resulted in the increase
230 of Granzyme B^+ $CD8^+$ and $KLRG1^+$ $CD8^+$ T cells and reduction of $Foxp3^+$ regulatory $CD4^+$ T
231 (Tregs) cells. IT MQ833 is more effective in reducing Tregs in both injected and non-injected
232 tumors than MQ832 (Fig. 2e,f, Extended Data Fig. 6a-c).
233
234 **MQ833-induced antitumor efficacy is dependent on STING/MDA5-mediated nucleus acid-**
235 **sensing pathways and STAT2-mediated type I IFN signaling pathway**
236 Given that MQ833 was designed to activate both the cytosolic DNA and dsRNA-sensing
237 pathways, we predict that its antitumor effects would be reduced in mice deficient of these
238 pathways. To test that, we implanted B16-F10 melanoma cells into the right flanks of WT,
239 *Sting*$^{Gt/Gt}$, *Mda5*$^{-/-}$, and *Sting*$^{Gt/Gt}$*Mda5*$^{-/-}$ mice. IT MQ833 resulted in 81% cure in WT mice and
240 45%, 46%, and 40% cure in *Sting*$^{Gt/Gt}$, *Mda5*$^{-/-}$, and *Sting*$^{Gt/Gt}$*Mda5*$^{-/-}$ mice, respectively (Fig. 2g,
241 h). These results indicate that both the cytosolic DNA and dsRNA-sensing pathways in the
242 tumor-bearing mice are important for IT MQ833-induced antitumor effects.
243
244 We have previously shown that type I IFN signaling pathway is important for rMVA (MQ710)-
245 induced antitumor effects. Here we found that tumor-bearing *Stat2*$^{-/-}$ mice also responded poorly
246 to IT MQ833 treatment (Fig. 2g, h) with only an 11% cure rate, confirming the importance of
247 IFNAR/STAT2 pathway in viral-induced antitumor immunity.
248

249 **Single-cell RNA sequencing (scRNA-seq) approach to interrogate the remodeling of tumor**
250 **immune microenvironment (TIME) after IT delivery of MQ833**
251 We next performed a series of scRNA-seq experiments to investigate the following questions: (i)
252 how does IT MQ833 alter TIME? (ii) what are the roles of nucleic acid-sensing and
253 IFNAR/STAT2 signaling pathways in regulating the transcriptomes of the myeloid and T cell
254 populations? and (iii) what is the role of IL-12 expressed in the MQ833-injected tumors in
255 modulating innate and adaptive immune responses?
256
257 In the first experiment, we sorted $CD45^+$ immune cells from B16-F10 tumors that had been
258 implanted intradermally in WT, *Sting*$^{Gt/Gt}$*Mda5*$^{-/-}$, and *Stat2*$^{-/-}$ mice, harvested at two days after
259 one dose of IT MQ833 and performed scRNA-seq analyses (Fig. 3a). Unsupervised clustering
260 revealed a total of 19 distinct clusters among the tumor-infiltrating $CD45^+$ immune cells,
261 including four T and NK cell clusters (C1-4), seven monocyte-macrophage clusters (C5-11), one
262 neutrophil cluster (C12), four DC clusters (C13-16), and one B cell cluster (C17). There are
263 small populations of undefined cells (C19) and melanoma cell contamination (C18) observed
264 (Fig. 3b,c). To verify our annotation for each cluster, we computed the expression score of a set
265 of known cellular markers for each cell type. Expression of markers for T cells (*Cd3d, Cd3g,*
266 *Trbc2*), regulatory T cells (*Foxp3, Tnfrsf4, Tnfrsf18*), NK cells (*Ncr1, Nkg7, Prf1, Xcl1, Gzma*),
267 DCs (*Itgax, H2-Eb1, Ccr7, Siglech, Wdfy4*), M2-like macrophages (*Apoe, C1qa, Mrc1, Pf4*),
268 M1-like macrophages (*Cxcl10, Chil3, Plac8, Ly6c2*), inflammartoy monocytes (*Fcgr1, Il18bp,*
269 *Ccl12, Ccl7*), and neutrophils (*S100a9, S100a8, Cxcl2*) correlated well with the cluster
270 annotation (Fig. 3c, Extended Data Fig. 7a).
271
272 We are particularly interested in the myeloid cell dynamics in an acute response to IT MQ833.
273 At two days post MQ833 injection, we observed rapid recruitment of inflammatory monocytes
274 (C5) and neutrophils (C12) into the injected tumors. The percentages of C5 and C12 out of
275 $CD45^+$ immune cells expanded from 1% to 29% and 0.3% to 12%, respectively (Fig. 3d, e). On
276 the other hand, the percentages of M2-like resident macrophages decreased from 13% to 0.6%,
277 whereas the percentages of M1-like macrophages increased from 8.3% to 17% (Fig. 3d,e). We
278 identified 4 DC clusters, cDC1, cDC2, pDC, and migrating DCs. The percentages of cDC1s in

279 the tumors were reduced from 4.7% to 0.5% after IT MQ833, suggesting that activation of cDC1
280 facilitates its migration to the draining lymph nodes (Fig. 3d,e).
281
282 IT MQ833 treatment on *Sting*$^{Gt/Gt}$*Mda5*$^{-/-}$ (DKO) resulted in the dramatic reduction of recruited
283 neutrophils compared with that in WT mice (2% in DKO vs. 12% in WT mice), modest
284 reduction of inflammatory monocytes recruitment (20% in DKO vs. 29% in WT mice), and less
285 efficient depletion of M2-like macrophages (6% in DKO vs. 0.6% in WT mice), although M1-
286 like macrophage polarization/activation was similar to that in WT mice (Fig. 3d,e). IT MQ833
287 reduced cDC1 from 6.2% to 2.1% in DKO mice, suggesting less efficient activation of cDC1 in
288 DKO mice compared with WT mice (Fig. 3d,e).
289
290 Tumor-infiltrating CD45^{+} immune cells in *Stat2*$^{-/-}$ mice showed some unique features compared
291 with WT mice. We observed two M2-like resident macrophage (C10) and M2-like proliferating
292 macrophage clusters (C11) unique to *Stat2*$^{-/-}$ mice in PBS mock-treated tumors. Upon IT MQ833
293 treatment, these two populations decreased from 21% to 0.1% and from 8.5% to 2% respectively.
294 By contrast, IT MQ833 resulted in a dramatic increase of M1-like macrophage (C9) in *Stat2*$^{-/-}$
295 mice from 0.7% to 46%, as well as an increase of neutrophils (C12) from 0.17% to 16.5% (Fig.
296 3d,e).
297
298 Gene set enrichment analysis (GSEA) of differentially expressed genes by CD45^{+} immune cells
299 sorted from MQ833-treated tumors vs. PBS mock-treated tumors revealed strong induction of
300 genes involved in the IFNA and IFNG responses and TNF signaling, followed by
301 IL6/JAK/STAT3 signaling, apoptosis, hypoxia, complement, IL2/STAT5 signaling pathways
302 (Fig. 3f,g). On the other hand, genes involved in oxidative phosphorylation and Myc targets are
303 downregulated after MQ833 injection (Fig. 3f,g).
304
305 Heatmap of the expression of genes involved IFNA and IFNG responses showed that IT MQ833
306 induced the expression of large array of IFN-stimulated genes in CD45^{+} immune cells from WT
307 mice and such responses were dramatically attenuated in DKO mice and absent in *Stat2*$^{-/-}$ mice
308 (Fig. 3h). For example, *Ifih1* (which encodes MDA5) was confirmed to be absent in CD45^{+} cells
309 from DKO mice. IT MQ833 induced the expression of Ifih1 in WT mice but not in *Stat2*$^{-/-}$ mice.

310 Similarly, *Zbp1* and *Adar* expressions were attenuated in DKO mice and absent in *Stat2*$^{-/-}$ mice.
311 Other examples with similar differential expression patterns include transcription factors *Stat2*
312 and *Irf7*, cytokines and chemokines such as *Cxcl10*, *Ccl7*, *Il6*, and *Il15*, and ISGs including
313 *Rsad2*, *Isg15*, *Ifit3, and Ifitm3*. *B2m* expression was reduced in DKO cells and absent in *Stat2*$^{-/-}$
314 cells (Fig. 3h).
315
316 Among all the cell clusters, neutrophils are one of the most heavily infected cells by MQ833
317 injection (Extended data Fig. 7b,c). Therefore, we sought to refine the analysis on the neutrophil
318 cluster. We analyzed differential gene expression in recruited neutrophils from WT mice after IT
319 MQ833 vs. PBS. *B2m*, *Isg15*, Gbp2, *Ifit3*, *Cxcl10*, and *Irf7* are among the top regulated genes
320 (Fig. 3i,j). The comparison of gene expression between neutrophils from WT and *Stat2*$^{-/-}$ mice
321 showed that neutrophils were sensitive IFN stimulation by expressing innate immune sensors,
322 cytokines and chemokines, ISGs and activation markers (Fig. 3i,j). Interestingly, MQ833
323 induced expression of antitumor-related genes from neutrophils such as *Ifng*, *Nos2*, *Fas*, *Il12a*,
324 *Cxcl1*, and *Cxcl10*, partially dependent on the MDA5/STING signaling pathway and
325 IFNAR/STAT2 positive feedback loop.
326
327 Collectively, these data demonstrate that IT MQ833 reprograms the tumor-infiltrating myeloid
328 cell compartment, by recruiting inflammatory monocytes and neutrophils, depleting M2-like
329 macrophages, and polarizing M1-like macrophages. IT MQ833 also activate neutrophils to
330 express antitumor genes including Nos2 in a MDA5/STING and STAT2-dependent fashion.
331
332 **IT MQ833 delivery remodels the T cell compartment of TIME**
333 We performed a sub-clustering analyses of CD3^{+} T cells from the same scRNA-seq dataset and
334 identified eight T-cell clusters including Tcf7^{+} Stem-like CD4^{+} T cells (C1), Tcf7^{+} progenitor T
335 cells (C2), Tcf7^{+}ISG^{hi}CD8 (C3), Early effector CD8 (C4), Effector CD8 (C5), Proliferating T
336 cells (C6), Th1 CD4 T cells (C7), and Tregs (C8) (Fig. 4a,b). C1 expressed *Tcf1*, *Il7r*, *Lars2, and*
337 low *CD4*, but no activation markers, representing stem-like CD4^{+} T cells in the tumors (Fig.
338 4c)[38]. C1 was enriched in PBS mock-treated tumors from *Stat2*$^{-/-}$ mice, which was reduced after
339 IT MQ833 (Fig. 4a,b). C2 expressed *Tcf7*, *Cd7*, *Klra7*, *Gzma*, but lacked CD4 and CD8
340 expression (Fig. 4a-c) and was designated as Tcf7^{+} progenitor T cells or CD8 Naïve-like[38]. C3

341 was designated as TCF^{+}ISG^{hi}CD8 because it expressed *Tcf7*, *Isg15*, *Ifit1*, *Ifit3*, but not *Gzma*,
342 *Gzmb* or *Ifng* (Fig. 4a-c). Overall, C1-C3 had the highest Tcf7 expression and had stem-like
343 features. C4 was designed as early effector CD8, because it not only expressed *CD8a*, *Ifg15*,
344 *Ifit3*, but also low levels of *Gmzb* and *Ifng*. C5 was designed as effector CD8 because it had the
345 highest expression of *Gzma*, *Gzmb* and *Ifng* among all of T cell subsets. C6 was designated as
346 proliferating CD8 T cells because it had the highest expression of *Mki67*, *Top2a*, *Hist1hib*. C7
347 expressed *CD4, Il7r, Cxcr6,* and *CD40lg* and was designed as Th1 CD4^{+} T cells. Finally, C8 was
348 designed as Tregs due to its expression of *CD4*, *Foxp3*, *Tnfrsf4* (encoding OX40), and *Tnfrsf18*
349 (encoding GITR) (Fig. 4a-c).
350
351 Upon IT MQ833, C1, C2, and C3 populations expressing *Tcf7* decreased from 5%, 37%, and
352 19% in the PBS mock-treated tumors to 1%, 10%, and 10%, respectively, in tumors from WT
353 mice, whereas Early effector CD8 (C4), Effector CD8 (C5) and Proliferating CD8 (C6) were
354 increased from 6.6%, 3.2%, 9.0% to 10%, 20%, and 28%, respectively (Fig. 4b-d). In tumors
355 from DKO mice, we observed an increase of C1 from 2% to 5%, a decrease of C3 from 21% to
356 15%, and no significant change of C2 (at 14%) upon MQ833 treatment (Fig. 4b-d). Early
357 effector CD8 (C4) decreased from 28% to 12% upon MQ833 treatment, while Effector CD8 (C5)
358 and Proliferating CD8 (C6) increased from 1.5% and 6.2% to 4.8% and 20.4% in DKO mice
359 (Fig. 4b-d). These results indicate that MQ833-induced differentiation of Tcf7^{+} stem-like T cells
360 and generation of Early effector CD8^{+} (C4) and Effector CD8^{+} T cells (C5) were attenuated in
361 DKO mice, whereas the generation of proliferating CD8^{+} T cells were not severely affected in
362 DKO mice.
363
364 In PBS mock-treated tumors from *Stat2*$^{-/-}$ mice, the Tcf7^{+} Stem-like CD4 T cells (C1) and Tcf7^{+}
365 progenitor T cells (C2) comprised of 51% and 15% of all CD3^{+} T cells respectively (Fig. 4b-d).
366 By contrast, Tcf7^{+}ISG^{hi}CD8 (C3), Early effector CD8 (C4), Effector CD8 (C5) were nearly
367 absent in tumors from *Stat2*$^{-/-}$ mice, indicating the essential role of type I IFN signaling in the
368 differentiation of Tcf7^{+} stem-like T cells into Tcf7^{+}ISG^{hi}CD8 (C3), Early effector CD8 (C4), and
369 Effector CD8 (C5) (Fig. 4b-d). Upon MQ833-treatment, C1 population was decreased from 51%
370 to 11% in *Stat2*$^{-/-}$ mice, proliferating CD8^{+} T cells (C6) population was increased from 6% to
371 27%, while C3, C4 and C5 were still absent, suggesting that in the absence of IFNAR/STAT2

372 signaling, (Fig. 4b-d), IL-12 alone cannot drive the differentiation of Tcf7$^+$ progenitor T cells
373 (C2) into transitory effector (C3 and C4) and effector CD8 T cells (C5). In addition, pseudotime
374 and cell trajectory analysis revealed a gradual shift of the T cell transcriptomic profile towards
375 decreased stemness and increased effector function and early exhaustion (Fig. 4e-f).
376
377 **scRNA-seq in bilateral B16-F10 tumor implantation model**
378 To gain a deeper understanding of the immune responses to MQ833 treatment in the injected and
379 non-injected tumors, we used the bilateral tumor implantation model in which the larger tumors
380 were injected with MQ833 twice three days apart, while the smaller tumors were not injected.
381 Two days after the second injection, we harvested both the injected and non-injected tumors and
382 performed scRNA-seq of tumor-infiltrating CD45$^+$ cells (Fig. 5a). Unsupervised clustering
383 revealed a total of 14 distinct clusters, including four T and NK cell clusters (C1-4), five
384 monocyte-macrophage clusters (C5-9), one neutrophil cluster (C10), three DC clusters (C11-13),
385 and one B cell cluster (C14) (Fig. 5b,c).
386
387 We observed an increase of neutrophil population (C10) from 0.65% in PBS mock-treated
388 tumors to 15% in tumors after two injections of MQ833 and to 0.5% in the contralateral non-
389 injected tumors (Fig. 5d,e). The inflammatory monocyte population (C5) increased from 1.8% in
390 PBS mock-treated tumors to 10.4% in the injected tumors and 12% in the non-injected tumors
391 (Fig. 5d,e). The M1-like macrophage population (C6) increased from 11% in PBS mock-treated
392 tumors to 16% in the injected tumors and 12% in the non-injected tumors, whereas the ISG$^+$
393 macrophage cluster (C7) increased from 0.3% to 4.8% in the injected tumors and 28% in the
394 non-injected tumors (Fig. 5d,e). By contrast, the M2-like macrophage population (C8) decreased
395 from 14.5% in PBS mock-treated tumors to 5.3% in the injected tumors and 2.5% in the non-
396 injected tumors (Fig. 5d,e). These results indicate that IT MQ833 resulted in extensive
397 remodeling of the TIME, with recruitment of neutrophils to the injected but not to the non-
398 injected tumors, expansion of ISG$^+$ macrophages and depletion of M2-like macrophages in both
399 the injected and non-injected tumors.
400
401 Sub-clustering analyses of CD3$^+$ T cells revealed a total of 9 clusters (Fig. 5f,g). Cluster 1
402 expressed *Tcf7*, *IL7r*, *Klf2*, and *Ikzf2* and lacked *Cd4* and *Cd8a* expression, which represent

403 Tcf7^{+} stem-like or progenitor T cells. Cluster 2 expressed *Cd8b1*, *Ccl5*, *Isg15*, *Ifit3*, *Tcf7*, and
404 *Zfp36l2*, representing Tcf7^{+}ISG^{hi}CD8^{+} T cells. Cluster 3 expressed *Cd8a*, *Itgb1*, *Dennd4a*, *Ccr5*,
405 and *Il2rb*, suggestive of resident memory CD8 T cells. Cluster 4 expressed *Cd8b1*, *Gzmb*, *Gzma*,
406 *Gzmk*, *Ifng*, *Ccl5*, and *Klrg1*, representing effector CD8 T cells. Cluster 5 expressed *CD8a*, *Tox*,
407 *Pdcd1*, *Havcr2*, *Nkg7*, *Klrd1*, and *Ifng*, representing stimulated CD8^{+} T cells expressing
408 exhaustion markers. Cluster 6 expressed *CD8a*, *Mki67*, *Top2a*, *His1h1b*, and *Ifng*, representing
409 proliferating CD8^{+} T cells. Cluster 7 expressed *CD4*, *Tcf7*, *Il7r*, *Ifit3*, and *Cd40lg*, representing
410 Th1 CD4 T cells. Cluster 8 expressed *Cd4*, *Foxp3*, *Tnfrsf4*, *Tnfrsf18*, representing Tregs. Cluster
411 9 expressed *Lyz2*, *CD74*, *Ifitm3*, *Fcer1g*, *Ms4a6c*, *H2-Ab1*, *H2-Aa*, *Cxcl2*, representing activated
412 CD3^{+} macrophages (Fig. 5f,g).
413
414 Upon IT MQ833, the Tcf7^{+} stem-like or progenitor T cells population (C1) decreased from 35%
415 in the PBS mock-treated tumors to 11.5% in MQ833-injected tumors and to 17% in MQ833-non-
416 injected tumors (Fig. 5h,i). Tcf7^{+}ISG^{hi}CD8^{+} T cells (C2) population decreased from 8.2% to
417 0.8% in the injected tumors and to 2.4% in the non-injected tumors (Fig. 5h,i). In addition,
418 Resident memory CD8^{+} T cells (C3) increased from 3.4% in the PBS-treated tumors to 7.3% in
419 the injected tumors and to 4% in the non-injected tumors (Fig. 5h,i). By contrast, Effector CD8^{+}
420 cells (C4) increased from 0.8% in PBS mock-treated tumors to 9% in injected tumors and to 26%
421 in the non-injected tumors, whereas Stimulated CD8^{+} T cells expressing exhaustion markers
422 (C5) increased from 1.1% to 27% in the injected tumors and to 2% in the non-injected tumors
423 (Fig. 5h,i). Proliferating CD8^{+} T cells (C6) also increased from 2.2% to 12.5% in the injected
424 tumors and 9% in the non-injected tumors (Fig. 5h,i). On the other hand, Th1 CD4^{+} T cells
425 expressing *Tcf7*, *Il7r*, and *Cd40lg* (C7) decreased from 33% to 7.4% in the injected tumors and
426 to 16% in the non-injected tumors (Fig. 5h,i). In addition, Tregs (C8) decreased from 11.8% to
427 4% in the injected tumors and 7.5% in the non-injected tumors (Fig. 5h,i). Finally, the unique
428 CD3^{+} population expressing macrophage markers (C9) expanded from 4.2% to 20% in the
429 injected tumors and to 16% in the non-injected tumors (Fig. 5h,i). These results indicate that
430 after two injections with MQ833, effector CD8^{+} T cells (C4) undergo expansion in the injected
431 tumors and perhaps trafficking to the non-injected tumors to elicit abscopal effects. Stimulated
432 CD8^{+} T cells expressing exhaustion markers (C5) became the largest population in the injected
433 tumors after IT MQ833.

434

435 **MQ833-induced antitumor efficacy requires both innate and adaptive immune systems**

436 To dissect the role of different immune cells in the MQ833-induced antitumor response, we
437 performed an antibody depletion study using the unilateral B16-F10 tumor implantation model.
438 Briefly, B16-F10 melanoma cells were implanted intradermally into the right flanks of
439 C57BL/6J mice. After the tumors were established, depleting antibodies for CD8 (anti-CD8),
440 CD4 (anti-CD4), NK (anti-NK1.1), neutrophils (anti-Ly6G), and macrophages (anti-CSF) were
441 delivered intraperitoneally twice weekly one day prior to IT MQ833. We measured tumor sizes
442 and monitor the survival of treated mice over time (Fig. 6a).

443

444 Flow cytometric analysis of peripheral blood confirmed the antibody depletion efficacy for anti-
445 CD4, CD8, NK1.1, and Ly6G (Extended Data Fig. 8a-c). Anti-CSF1 antibody has been shown to
446 deplete macrophages in the tumors[39]. MQ833 treatment alone yielded 55% survival rate. $CD8^+$ T
447 cell depletion abrogated the antitumor effects resulting in no survivors, but extended the median
448 survival from 11.5 days in PBS mock-treated mice to 30.5 days in MQ833 + αCD8 group ($p <$
449 0.0001), suggesting that other immune cells also contribute to virus-induced antitumor efficacy
450 (Fig. 6b,c). To our surprise, neutrophil depletion significantly impaired the overall therapeutic
451 efficacy, resulting in 10% survival with a medium survival of 24 days ($p < 0.0001$; PBS vs.
452 MQ833 + αLy6G) (Fig. 6b,c). Macrophage depletion with αCSF1 also resulted in attenuated
453 antitumor effects with a 10% survival rate with a median survival of 34.5 days ($p < 0.0001$; PBS
454 vs. MQ833 + αCSF1) (Fig. 6b,c). Depleting $CD4^+$ T cells or NK cells did not negatively impact
455 the antitumor efficacy (Fig. 6b,c), although we have previously shown $CD4^+$ T cells are critical
456 for generating memory T cell responses in the setting of virus-induced antitumor immunity[17].
457 Collectively, these findings demonstrate that MQ833-induced antitumor immunity requires both
458 innate and adaptive immunity, and that $CD8^+$ T cells, neutrophils, and macrophages are the most
459 crucial players.

460

461 ***Nos2* is required for MQ833-induced antitumor effects**

462 The role of inducible nitric oxide synthase (iNOS or Nos2) in promoting or restricting tumor
463 growth is complicated and context-dependent[40, 41]. Here we analyzed iNOS protein expression in
464 neutrophils and macrophages in tumors harvested two days after second injection (Fig. 6d) using

465 flow cytometry analysis. We observed that intracellular iNOS protein levels were strongly
466 induced in tumor-infiltrating neutrophils and M1-like macrophages and was reduced in $CD206^+$
467 M2-like macrophages upon MQ833 treatment (Fig. 6e).
468
469 To determine whether *Nos2* is required MQ833-induced antitumor effects, we implanted B16-
470 F10 melanoma into the right flanks of *Nos2*$^{-/-}$ mice and age-matched WT C57BL/6J mice.
471 Tumors were treated with IT MQ833 twice weekly or PBS as a control. IT MQ833 resulted in
472 50% cure rate in WT mice and only 10% cure rate in *Nos2*$^{-/-}$ mice (Fig. 6g,h). IT MQ833
473 extended the medium survival from 14 days in PBS mock-treated mice to 61 days in WT mice (p
474 < 0.0001). However, in *Nos2*$^{-/-}$ mice, IT MQ833 extended the medium survival from 17 days to
475 in PBS mock-treated mice to 40 days ($p = 0.0003$). In PBS mock-treated mice, *Nos2*$^{-/-}$ mice died
476 3 days later than their WT controls ($p = 0.029$). Our results indicate that *Nos2* is required for
477 MQ833-induced antitumor effects, but in the absence of viral treatment, *Nos2* plays a pro-tumor
478 role. To rule out the requirement for *Nos2* is specific for B16-F10 melanoma model, we
479 compared the therapeutic efficacy of IT MQ833 for MC38 murine colon cancer in *Nos*$^{-/-}$ and age-
480 matched WT mice. We observed that IT MQ833 generated 100% cure in WT mice but reduced
481 efficacy in *Nos*$^{-/-}$ mice (Extended Data Fig. 4f,g).
482
483 To address how MQ833 regulates Nos2 expression, we first examined whether IL-12 expression
484 by MQ833 contributes to *Nos2* gene expression. scRNA-seq analysis of $CD45^+$ immune cells
485 sorted from tumor samples harvested at 2 days post one injection of MQ833, rMVAΔE3L, or
486 PBS were performed. Unsupervised clustering analysis revealed a total of 14 clusters. MQ833
487 and rMVAΔE3L treatment reduced M2-like macrophages from 16% to 3.4% and 5%,
488 respectively and increased inflammatory monocytes from 0.7% to 25% and 30%, respectively.
489 MQ833 and rMVAΔE3L treatment also increased neutrophils from 0.3% to 13% and 18%,
490 respectively (Extended data Fig. 9a-c).
491
492 $CD3^+$ T cell sub-clustering analysis revealed that upon MQ833 and rMVAΔE3L treatment,
493 $TCF7^+$ Stem-like T cells (C1) decreased from 32% to 2% and 7% respectively (Extended data
494 Fig. 9d-g). The most striking difference is that C5 population (expressing *Lars2*, *Vps37b*, *Satb1*,
495 *Plac8*, *Emb*, *Dennd4a*) increased from 0.2% to 40% in MQ833-treated tumors and remained

496 unchanged in rMVAΔE3L-treated tumors. In addition, C7 population (expressing *Nkg7*, *Lag3*,
497 *Ifng*, *Cxcr6*, *Ccl4*, *Gzmb*) also increased from 6% to 13.6% in MQ833-treated tumors and
498 decreased to 4% in rMVAΔE3L-treated tumors. By contrast, C6 population (expressing *Mki67*
499 and other cell proliferation markers) increased from 4.7% to 12% and 10.5% after MQ833 and
500 rMVAΔE3L treatment, respectively. These results suggest that IL12-expressing MQ833 is more
501 efficient in promoting the expansion of effector memory $CD8^+$ and effector $CD8^+$ T cells than
502 rMVAΔE3L.
503
504 We hypothesized that the IL-12-expressing MQ833 might be more efficient in inducing *Nos2*
505 expression in activated neutrophils and M1-like macrophages than rMVAΔE3L due to its
506 enhanced ability to induce IFN-γ production by $CD8^+$ T cells. Indeed, *Nos2* expression was
507 upregulated in neutrophils and M1-like macrophages after IT MQ833 treatment (Fig. 6i).
508 Heatmap of differential gene expression involved in antitumor activities showed that MQ833
509 treatment was more effective than rMVAΔE3L in inducing *Fas*, *Tnf*, *Ifng*, *Nos2*, *Cxcl10* in
510 CD45, neutrophils, M1-like macrophages and monocytes in the tumor microenvironment (Fig.
511 6j). Flow cytometry analysis revealed that iNOS expression in neutrophils was reduced in
512 MQ833-treated tumors from *Stat1*$^{-/-}$ mice compared with WT controls, suggesting that IFNGR
513 signaling might also play a role in iNOS induction. Taken together, our results suggest that the
514 nucleic sensing pathways, and IFNAR and IFNGR signaling on neutrophils might be important
515 for promoting iNOS expression and ultimately the production of nitric oxide for tumor cell
516 killing.
517
518 **IT MQ833 delays tumor growth in the absence of adaptive immune system**
519 We used a *Rag1*$^{-/-}$ mouse model to test whether IT MQ833 generates antitumor effects in the
520 absence of mature T and B cells. Briefly, B16-F10 melanoma cells were implanted intradermally
521 into the right flanks of *Rag1*$^{-/-}$ and age-matched WT controls. When the tumors grew to 3 mm in
522 diameter, they were injected with MQ833 (4×10^7 pfu) twice weekly or with PBS as mock
523 treatment controls (Fig. 7a). IT MQ833 generated 10% cure in *Rag1*$^{-/-}$ mice and extended the
524 medium survival from 11 days in the PBS mock-treatment control to 42 days in the treatment
525 group ($p < 0.0001$; Fig. 7b, c). Flow cytometry analysis of tumor-infiltrating myeloid cells in
526 *Rag1*$^{-/-}$ mice revealed that more than 55% $CD45^+$ cells in the MQ833-injected tumors were

527 neutrophils compared with 1.8% in PBS mock-injected tumors, and 31% of them expressed
528 iNOS (Fig. 7d, e). These results indicate that MQ833-induced neutrophil recruitment and
529 activation is independent of mature T and B cells and IT MQ833 delays tumor growth in mice
530 lacking adaptive immune system.
531
532 **MQ833 cures B16-F10 tumor lacking MHC-I**
533
534 Mutations in MHC Class I antigen presentation machinery have been observed in the tumors
535 of patients that relapse after initial response to immune checkpoint blockade (ICB)[42, 43,44]. Beta-2
536 microglobulin (B2M) is a component of the MHC-I molecule and is essential for MHC-I antigen
537 presentation and B2M loss or downregulation is associated with acquired resistance to ICB
538 therapy in melanoma patients[43, 44]. B2M-loss tumors are resistant to $CD8^+$ T cell mediated
539 killing. Given that IT MQ833 generated antitumor effects independent of $CD8^+$ T cells, we
540 wonder if it could have therapeutic effects in *B2m*$^{-/-}$ tumors. To test that, we generated a *B2m*$^{-/-}$
541 B16-F10 cell line using CRISPR-cas9 and they were implanted intradermally into the right
542 flanks of WT C57BL/6J mice. After the tumors were established, they were treated with either
543 MQ833, MQ832, or PBS. IT MQ833 treatment eradicated 70% of the *B2m*$^{-/-}$ tumors, whereas IT
544 MQ832 resulted no cure (Fig. 7f, g). When we rechallenged the survivors with a lethal dose WT
545 B16 tumor cells two months later, all of the mice rejected the tumor rechallenge, indicating a
546 long-lasting memory response induced by MQ833 treatment (Fig. 7h). These results highlight the
547 potential application of MQ833 in treating ICB-resistant tumors in patients.
548

549 **Discussion**

550

551 Viral-based cancer immunotherapy has the potential to remodel the tumor immune
552 microenvironment (TIME) to overcome both primary and acquired resistance to ICB therapy. In
553 general, virus infection of tumor and immune cells activates the innate immune system, induces
554 cell death, and promotes antigen-specific T cells. In this study, we engineered an immune-
555 activating recombinant MVA, MQ833, by deleting three immune-suppressive genes (E3L, E5R,
556 and WR199) and inserting three transgenes (Flt3L, OX40L and IL-12). We provided evidence
557 that our stepwise engineering of the virus through rational design improves antitumor immunity.
558 Using antibody depletion, we determined that MQ833-induced antitumor effects are dependent
559 on $CD8^+$ T cells, activated neutrophils, and M1-like macrophages. Using genetically engineered
560 mice deficient in the nucleic acid-sensing pathways and type I IFN signaling, we demonstrated
561 that MQ833 activates the MDA5 and STING-dependent cytosolic dsRNA and DNA-sensing
562 pathways and STAT2-dependent type I IFN signaling. More importantly, using single-cell RNA-
563 seq technology, we examined how IT MQ833 altered the tumor-infiltrating immune cell
564 populations and transcriptomes at a single-cell level.

565 Based on our results, we proposed the following working model illustrating the mechanisms of
566 action of MQ833 (Fig. 7i). Infection of tumor and immune cells with MQ833 results in the
567 induction of type I IFN and proinflammatory cytokines and chemokines in the tumor
568 microenvironment via the MDA5/STING pathway. Localized IL-12 expression by MQ833-
569 infected cells in the presence of type I IFN further promotes the differentiation of $Tcf7^+$ stem-
570 like CD8 and CD4 T cells into early effector and effector T cells as well as stimulating IFN-
571 γ production, which is important for polarization of M1-like macrophages. Upon MQ833
572 infection, neutrophils are recruited to the injected tumors and activated by the combination of
573 cytosolic nucleic acid-sensing pathway and IFNAR/IFNGR signaling to produce nitric oxide via
574 iNOS, which results in tumor killing.

575 IL-12 is a pleiotropic cytokine important for stimulating T and NK cells. Because systemic
576 delivery of IL-12 causes toxicity[45, 46], we engineered MQ833 to express extracellular matrix-
577 anchored IL-12 to stimulate intratumoral T cells and perhaps NK cells. The function of IL-12
578 was assessed by comparing the antitumor efficacy of MQ833, in which an IL-12 expression

579 cassette was inserted into the WR199 locus, with MQ832 in which WR199 was depleted but no
580 transgene was added. In both WT B16-F10 murine melanoma and MC38 murine colon cancer
581 models, IT MQ833 is more effective than MQ832, which correlates with stronger activation of
582 $CD8^+$ T cells and more profound reduction of Tregs.

583 scRNA-seq analyses of tumor-infiltrating T cells provided insights into how T cell subsets
584 undergo profound changes upon IT MQ833 treatment. Tcf7 encodes a transcription factor TCF1
585 important for maintaining stem-like memory T cells during chronic virus infection and in
586 tumors[47, 48, 49]. We observed that $Tcf7^+$ stem-like T cells gradually lost Tcf1 expression and
587 gained expression of ISGs and effector T cell markers. Such differentiation program was
588 attenuated in *Sting*$^{Gt/Gt}$*Mda5*$^{-/-}$ mice and absent in *Stat2*$^{-/-}$ mice, highlighting the importance of
589 type I IFN production and signaling in promoting differentiation of intratumoral $Tcf7^+$ stem-like
590 T cell towards effector T cells upon virotherapy.

591 Our study also demonstrated that MQ833 could exert $CD8^+$ T cell-independent antitumor effects,
592 likely through the actions of activated neutrophils and M1-like macrophages. First, depleting of
593 $Ly6G^+$ neutrophils using anti-Ly6G antibody or abrogating macrophages using anti-CSF1
594 antibody resulted in a dramatic reduction of therapeutic efficacy. Secondary, IT MQ833 delays
595 tumor growth in *Rag1*$^{-/-}$ mice, lacking mature T and B cells. Third, IT MQ833 cured B2m-null
596 B16-F10 cells, resistant to CD8-mediated tumor killing. Analyses from multiple scRNA-seq
597 datasets revealed that IT MQ833 promoted neutrophil recruitment and activation, depleted M2-
598 like macrophages, and polarized M1-like macrophages for antitumor effects. Because MHC I
599 loss is a frequent cause of acquired resistance to ICB therapy, we propose that MQ833 provides
600 an effective alternative to mobilize and activate myeloid cells for generating antitumor effects.

601 Neutrophils are one of the most abundant myeloid cells derived from granulocyte-monocyte
602 progenitors (GMP) in the bone marrow. They provide the first line of defense when encountering
603 pathogens such as bacteria and viruses. They can also be recruited to sites of injury and play a
604 role in tissue repair[50]. The role of neutrophils in tumor immunity is complex[51, 52, 53, 54].
605 Neutrophils can be expanded in response to immune mediators from growing tumors and play a
606 pro-tumor role in tumor progression and metastasis[55, 56]. Similar to the M1 and M2 dichotomy of
607 tumor-associated macrophages (TAMs), tumor-associated neutrophils (TANs) can be classified

608 into anti-tumor N1 and pro-tumor N2 based on their functional status. It has been shown that
609 TGF-β blockade results in the recruitment and activation of TANs towards N1 polarization[57].
610 Neutrophils are recruited to the sites of radiation and contribute to antitumor responses[58]. In
611 addition, concurrent administration of G-CSF enhanced RT-mediated antitumor activity[58].

612 In our study, IT MQ833 resulted in the recruitment and activation of neutrophils two days post
613 injection. scRNA-seq analyses of neutrophils in tumors from WT mice treated with MQ833
614 showed a strong IFN signature, which is attenuated in *Sting*$^{Gt/Gt}$*Mda5*$^{-/-}$ mice and abolished in
615 *Stat2*$^{-/-}$ mice. In addition, IT MQ833 induced neutrophils from WT mice to express genes
616 involved in antitumor activities, including *Fas*, *Il12a*, *Ifng*, *Nos2*, *Cxcl1* and *cxcl10*. By contrast,
617 IT MQ833 induced neutrophils from *Stat2*$^{-/-}$ mice to induce genes involved in pro-tumor
618 functions, including *Arg1*, *Mmp9*, *Elane*, and *Il1b*. These results support that treatment with
619 immunogenic virus induces TAN polarization to N1 phenotype which is dependent on type I IFN
620 signaling.

621 In this study, we showed that neutrophil recruitment is independent of mature T and B cells after
622 MQ833 treatment, which contributed to the therapeutic effects in *Rag1*$^{-/-}$ mice. These findings
623 have important pre-clinical and clinical implications. First, hMQ833 may potentially be tested in
624 patient-derived xenograft (PDX) models for antitumor effects in immune-deficient mice prior to
625 clinical administration; Second, hMQ833 can be used in immune-compromised patient
626 populations in which T or B cells are dysfunctional or depleted.; and lastly, hMQ833 can be
627 safely administered to these patients due to the non-replicative nature of the virus.

628 In summary, through rational design, we engineered a second generation recombinant MVA
629 (MQ833) for cancer immunotherapy either as monotherapy or in combination with ICB. MQ833
630 is replication incompetent but can profoundly remodel TIME to promote both innate and
631 adaptive antitumor immunity through (i) recruitment and activation of neutrophils, (ii) depletion
632 of suppressive cells such as Tregs and M2-like macrophages, and (iii) expansion of M1-like
633 macrophages, effector memory and effector T cells. Finally, our results suggest that IT MQ833
634 can be used effectively in patients with primary or acquired resistance to ICB.

635 **Methods**

636

637 **Mice**

638 Female C57BL/6J mice between 6 and 8 weeks of age were purchased from the Jackson
639 Laboratory (Strain #000664) were used for the preparation of bone marrow-derived dendritic
640 cells and for *in vivo* experiments. These mice were maintained in the animal facility at the Sloan
641 Kettering Institute. All procedures were performed in strict accordance with the
642 recommendations in the Guide for the Care and Use of Laboratory Animals of the National
643 Institutes of Health. The protocol was approved by the Committee on the Ethics of Animal
644 Experiments of Sloan Kettering Cancer Institute. *Sting*$^{Gt/Gt}$ mice were generated in the laboratory
645 of Dr. Russell Vance (University of California, Berkeley). *cGas*$^{-/-}$ (Strain # 026554), *Stat1*$^{-/-}$
646 (Strain # 012606), *Stat2*$^{-/-}$ (Strain #023309) and *Nos2*$^{-/-}$ (Strain #002609) mice were purchased
647 from Jackson Laboratory. *Mda5*$^{-/-}$ mice were generated in Marco Colonna's laboratory
648 (Washington University)[59]. *Mda5*$^{-/-}$*Sting*$^{Gt/Gt}$ were bred in our lab[60].

649

650 **Cell lines**

651 BHK-21 (baby hamster kidney cell, ATCC CCL-10) cells were cultured in Eagle's minimal
652 essential medium containing 10% fetal bovine serum (FBS), 0.1 mM nonessential amino acids,
653 penicillin, and streptomycin. The murine melanoma cell line B16-F10 was originally obtained
654 from I. Fidler (MD Anderson Cancer Center). The MC38 cell line was obtained from ATCC.
655 The B16-F10 cell line was maintained in RPMI-1640 medium supplemented with 10% FBS,
656 0.05 mM 2-mercaptoethanol, penicillin, and streptomycin. The B16-F10 cell line lacking B2M
657 gene were generated by using CRISPR-cas9 technology.

658

659 **Viruses**

660 The MVA virus was a kind gift from Gerd Sutter (University of Munich). MVAΔE5R,
661 MVAΔE5R-hFlt3LmOX40L (rMVA or MQ710), rMVAΔE3L, rMVAΔE3LΔWR199 (MQ832),
662 rMVAΔE3LΔWR199-IL12 (MQ833), and hMQ833 were generated by transfecting pUC57-
663 based plasmids into BHK-21 cells that were infected with MVA at MOI 0.05. Recombinant
664 viruses were purified after 4~6 rounds of plaque selection based on the fluorescence marker.

665 PCR and DNA sequencing were performed to verify the purity of the recombinant viruses.
666 Viruses were propagated in BHK-21 cells and purified through a 36% sucrose cushion.
667
668 **Human monocyte-derived dendritic cell (moDC) generation and T cell isolation**
669 All collection and use of human specimens adhered to protocols reviewed and approved by the
670 Institutional Review and Privacy Board of Memorial Hospital, MSKCC. Buffy coat products
671 were obtained from healthy donor at New York Blood Center and peripheral blood mononuclear
672 cells (PBMCs) separated by standard centrifugation over Ficoll-Paque PLUS (Amersham
673 Pharmacia Biotech, Uppsala, Sweden). Tissue culture plastic adherent PBMCs comprised the
674 moDCs precursors, which were cultured in complete PRMI 1640-1% human serum
675 supplemented with 1000 IU/ml GM-CSF (PeproTech) and 500 IU/ml IL-4 (PeproTech).
676 Fresh medium and cytokines were replenished every 48 h. T cells were obtained from tissue
677 culture nonadherent PBMCs, then further purified by $CD8^+$ T cell or $CD4^+$ T cell isolation kit
678 (Miltenyi Biotec) following manufacturer's instruction.
679
680 **Tumor processing and flow cytometry staining**
681 Tumor samples were collected in cold RPMI and thoroughly chopped into small pieces with
682 surgical scissor. Then we added Liberase TL (1.67 Wünsch U/ml) and DNase I (0.2 mg/ml) to
683 the tube and incubated in 37 °C shaker for 20-30 minutes. Digested tumors were then transferred
684 to GentleMACs C Tube and homogenized using the Gentle MACs Octo Dissociator (Miltenyi
685 Biotec) according to manufacturer's instruction. Samples were then filtered through 70 um filter
686 and quenched with 10 ml cold PBS and spun down. Cells were then washed with MACS buffer
687 (Miltenyi Biotec) twice, and stained with Fc block (BD), viability dye eFluor506 (eBioscience),
688 and cell surface antibodies diluted in MACS buffer for 30 minutes on ice in the dark, and
689 subsequently fixed and permeabilized using the Foxp3 fixation and permeabilization kit (Thermo
690 Fisher). Cells were then incubated with intracellular antibodies diluted in permeabilization buffer
691 for 30 minutes or overnight.
692 The following antibodies were used for flow cytometric staining: CD45 Pacific blue (clone 30-
693 F11, Biolegend), CD3 BUV395 (clone 145-2C11, BD), CD4 BUV737 (clone RM4-5, BD), CD8
694 Alexa Fluor 700 (clone 53-6.7, Biolegend), OX40 BV605 (clone OX-86, Biolegend), TIM3
695 BV711 (clone RMT3-23, Biolegend), PD-1 AF647 (clone RMPI-30, BD), KLRG1 APC-Cy7

696 (clone 2F1/KLRG1, Biolegend), Foxp3 PerCP-Cy5.5 (clone FJK-16s, Invitrogen), Ki67 BV786
697 (clone B56, BD), TOX PE (clone REA473, Miltenyi Biotec), Granzyme B PE-Texas red (clone
698 GB11, Invitrogen), CD11b APC-eFluor780 (clone M1/70, eBioscience), Ly6G PE-Cy7 (clone
699 1A8, BD), F4/80 APC (clone BM8, Biolegend), CD68 BV421 (clone FA-11, Biolegend), iNOS
700 PE (clone W16030C, Biolegend).
701
702 After staining, cells were washed and resuspended with MACS buffer and transferred into FACS
703 tubes with 70 um filter caps. Single cell suspensions were run on Cytek Aurora analyzer, and the
704 data was analyzed with Flowjo.
705
706 **Generation of bone marrow-derived dendritic cells**
707 Bone marrow cells were extracted from the femur and tibia of mice. After centrifugation, cells
708 were re-suspended in ACK Lysing Buffer (Lonza) for red blood cell lysis by incubating the cells
709 on ice for 1-3 min. Cells were then resuspended in fresh medium and filtration through a 70-µm
710 cell strainer (BD Biosciences). For the generation of Flt3L-BMDCs, the bone marrow cells (5
711 million cells in each well of 6-well plates) were cultured in complete medium (CM) in the
712 presence of Flt3L (100 ng/ml; R & D systems) for 7–9 days. Cells were fed every 2–3 days by
713 replacing 50% of the old medium with fresh medium. For the generation of GM-CSF-BMDCs,
714 the bone marrow cells (5 million cells in each 15 cm cell culture dish) were cultured in RPMI-
715 1640 medium supplemented with 10% fetal bovine serum (FBS) in the presence of 30 ng/ml
716 GM-CSF (BioLegend) for 9-12 days. Fresh medium and cytokine were replenished every 2-3
717 days.
718
719 **RNA isolation and Real-time PCR**
720 Cells were infected with various viruses at a MOI of 10 for 1 hour or mock-infected. The
721 inoculum was removed, and the cells were washed with PBS twice and incubated with fresh
722 medium for 16 hours or overnight. RNA was extracted from whole-cell lysates with RNeasy Plus
723 Mini kit (Qiagen) and was reverse-transcribed with cDNA synthesis kit (Thermo Fisher). Real-
724 time PCR was performed in triplicate with SYBR Green PCR Master Mix (Life Technologies)
725 and Applied Biosystems 7500 Real-time PCR Instrument (Life Technologies) using gene-

726 specific primers. Relative expression was normalized to the levels of glyceraldehyde-3-
727 phosphate dehydrogenase (GAPDH).
728
729 **ELISA**
730 For IL-12 transgene expression verification, B16 cells were infected with MVAΔE5R or MQ833
731 at a MOI of 10 for 1 hour. Mock-infected cells were used as a control. The supernatant was
732 removed, and the cells were washed with PBS twice and incubated with fresh medium for 16
733 hours. Supernatant was collected from the culture, and IL-12 levels were determined using
734 Duoset ELISA kit (R&D) following manufacturer's instruction.
735 For T cell activation assays, supernatant from the co-culture system were collected and IFNγ
736 levels were determined by Duoset ELISA kit (R&D).
737
738 **ELISPOT assay**
739 Spleens were harvested from mice treated with different viruses and were mashed through a
740 70 μm strainer (Thermo Fisher Scientific). Red blood cells were lysed using ACK Lysis Buffer
741 (Life Technology), and the cells were then resuspended in RPMI medium. Enzyme-linked
742 ImmunoSpot (ELISPOT) assay was performed to measure IFN-γ+ CD8+ T cells, according to
743 the manufacturer's protocol (BD Bioscience). 1×10^6 splenocytes were co-cultured with 2.5×10^5
744 irradiated B16-F10 in complete RPMI medium overnight. IFNγ+ splenocytes were detected by
745 Mouse IFNγ ELISPOT kit (BD Biosciences)
746
747 **Western blot analyses**
748 B16-F10 cells or BMDCs were infected with MQ832 or MQ833 at a MOI of 10 for 1 hour.
749 Mock-infected cells were used as a control. Cells were then washed with PBS twice and cultured
750 with fresh medium. Cells were lysed in RIPA lysis buffer supplemented with 1x Halt™ Protease
751 and Phosphatase Inhibitor Cocktail at indicated time points. Protein samples were separated by
752 SDS-PAGE and then transferred to nitrocellulose membrane. Primary antibodies specific for
753 phospho-IRF3 (1:500, CST, 4947), IRF3 (1:1000, CST, 4302), cGAS (1:1000, CST, 31659),
754 STING (1:1000, CST, 13647), phospho-STING (1:500, CST, 72971), TBK1 (1:1000, CST,
755 3504), MDA5 (1:500, CST, 5321) and phospho-TBK1 (1:500, CST, 5483) were used. GAPDH
756 antibody (1:5000, CST, 2118) were used as loading controls. Anti-rabbit HRP-linked IgG

757 antibody was used as a secondary antibody (1:5000, CST, 7074). Detection was performed using
758 SuperSignalTM Substrates (Thermo Fisher, 34096 or A38555).
759
760 **In vitro T cell activation assay**
761 For murine MQ833, splenic CD11c+ DCs were sorted from WT mice and subsequently infected
762 with various viruses at a MOI of 10 for 1 hour and pulsed with OVA (1.25 mg/ml). OT-1 T cells
763 were isolated from the spleens OT-1 mice using negative selection with $CD8a^+$ T Cell Isolation
764 Kit (Miltenyi Biotec) according to the manufacturer's instructions. OT-1 T cells were then co-
765 cultured with DCs (DC:T = 1:3) for 3 days. Alternatively, T cells were incubated with
766 supernatant collected from the infected $CD11c^+$ DCs for 3 days. IFN-γ levels in the supernatants
767 were determined by ELISA.
768
769 For human MQ833, human moDCs were infected with various viruses at a MOI of 10 for 1 hour
770 and pulsed with OVA (1.25 mg/ml). CD8 or CD4 T cells were purified from human PBMCs
771 using isolation kits (Miltenyi Biotec) following manufacturer's instruction. T cells and moDCs
772 were co-cultured (DC:T = 1:5) for 3 days and supernatant were then collected for IFN-γ ELISA.
773
774 **Generation of $B2m^{-/-}$, $Sting^{-/-}$, $Mda5^{-/-}Sting^{-/-}$ B16-F10 cells**
775 B16-F10 cells were transfected with plasmids for expression of Cas9 and gRNAs against B2M.
776 Two gRNA expression plasmids targeting exon 2 of B2M were co-transfected. Plasmid
777 backbones used to create these CRISPR constructs were created by the Church group and
778 obtained from Addgene (Mali et al 2013). After transfection, cells were induced to express the
779 complex MHC class I by treating with 100 units of interferon gamma for 2 days. Afterwards,
780 cells were dissociated with trypsin and staining antibody against H-2Kb-PE (BD, AF6-88.5). The
781 MHC class I complex (including H-2Kb) requires B2M to be stable on the surface of cells.
782 Single cells that were negative for surface MHC-I were sorted onto 96 well plates. Single cells
783 were then expanded to produce clonal isolates. After outgrowth of clones, PCR using primers
784 specific to the B2M locus was used to confirm which isolates contained a deletion of B2M
785 (between the two gRNA target sites). The same PCR products were also cloned into TopoTA
786 plasmids for sequencing. A subsequent western blot confirmed loss of B2M protein using an

787 antibody against B2M protein (Abcam 75853). PCR, DNA sequencing, and western blot all
788 confirmed loss of B2M.
789
790 Sting$^{-/-}$ and Mda5$^{-/-}$Sting$^{-/-}$ B16-F10 cells were generated similarly to the B2m$^{-/-}$ except that
791 instead of sorting, transfected cells were isolated by limiting dilution. Lesions at the target sites
792 were confirmed by PCR amplification and T7 endonuclease assay.
793
794 **Tumor challenge and treatment**
795 For flow cytometric analysis and single cell RNA-seq, 5×10^5 B16-F10 tumor cells were
796 implanted intradermally into the right flanks of the mice for the unilateral tumor implantation
797 model. For bilateral implantation, 5×10^5 and 2.5×10^5 B16-F10 tumor cells were implanted
798 intradermally into the right and left flanks of mice. At 8-11 days after implantation when tumors
799 were established, the tumors at the right flank were injected with 4×10^7 PFU of MQ832,
800 MQ833, or PBS once, or twice with 3 days apart. Tumors were harvested two days after second
801 injection.
802
803 For survival experiments, 5×10^5 B16-F10 cells or 1×10^6 B2m$^{-/-}$ B16 cells were implanted
804 intradermally into the shaved skin on the right flanks of WT C57BL/6J mice or age-matched
805 *cGas*$^{-/-}$, *Sting*$^{Gt/Gt}$, Mda5$^{-/-}$, *Sting*$^{Gt/Gt}$*Mda5*$^{-/-}$, and *Stat2*$^{-/-}$ mice. Once the tumors are 3 mm in
806 diameter or larger, they were injected with 4×10^7 PFU of MQ832, MQ833 or PBS when the mice
807 were under anesthesia. Viruses were injected twice weekly as specified in each experiment and
808 tumor sizes were measured twice a week. For combination therapy with ICBs, the following
809 antibodies were injected interperitoneally twice weekly: anti-CTLA-4 (100 µg per mouse), Anti-
810 PD-L1 (200 µg per mouse), anti-PD-1 (200 µg per mouse), or isotype control antibody. Tumor
811 volumes were calculated according to the following formula: l (length) × w (width) × h
812 (height)/2. Mice were euthanized for signs of distress or when the diameter of the tumor reached
813 10 mm.
814
815 In the bilateral tumor implantation model, B16-F10 cells were implanted intradermally into right
816 (5×10^5) and left (1×10^5) flanks of C57BL/6J mice. After 7 days after implantation when the

817 tumors were established, the tumors at the right flank were injected with 4×10^7 PFU of MQ832,
818 MQ833 or PBS twice weekly.
819
820 For the tumor rechallenge study, the survived mice (more than 60 days after initiation of
821 intratumoral virotherapy) were rechallenged with intradermal delivery of a lethal dose of B16-
822 F10 or B2m KO B16-F10 (1×10^5 cells) at the contralateral side.
823
824 **Purification of anti-CSF-1 monoclonal antibody**
825 The anti-CSF-1 monoclonal antibody (clone 5A1) was purified from cell supernatant of
826 hybridoma (ATCC, #CRL-2702)[61, 62]. Briefly, hybridoma cells were cultured in Hybridoma-SFM
827 medium (Thermo #12045076) for 3 weeks to produce antibody. Cell supernatant was collected to
828 do antibody purification by using LigaTrap Rat IgG purification column (LigaTrap Technologies
829 #LT-138) according to the manufacturer's procedure. Antibody quality and concentration were
830 examined by SDS-PAGE gel electrophoresis and nanodrop, respectively.
831
832 **In vivo antibody depletion experiment**
833 Immune cell subsets were depleted by administering 200 μg monoclonal antibodies i.p. twice
834 weekly starting 1 day prior to the first viral injection as indicated, continued until the animals
835 either died, were euthanized, or were completely clear of tumors: anti-CD8-α for CD8+ T cells
836 (clone 2.43, BioXCell), anti-CD4 for $CD4^+$ T cells (clone GK1.5, BioXCell), anti-NK1.1 for NK
837 cells (clone PK136, BioXCell). 500 μg of anti-Ly6G (clone 1A8, BioXCell) were given for
838 neutrophil depletion. 500 μg of anti-CSF1 (provided by Ming Li's laboratory) were given every
839 5 days for macrophage depletion. Depletion efficacies of CD8 T cells, CD4 T cells, NK cells and
840 neutrophils were confirmed by flow cytometry of peripheral blood. (Extended Data Fig. 8)
841
842 **Cell sorting for tumor infiltrating immune cells**
843 Tumors were harvested and single cell suspensions were prepared. Cells were then stained with
844 Cell Viability Dye eFluor506 (eBioscience) and anti-CD45 antibody Pacific blue (clone 30-F11,
845 Biolegend). $CD45^+$ live cells were then sorted using BD Aria cell sorter.
846
847 **Single-cell RNA-sequencing and data analysis.**

848 *Library preparation and sequencing*

849 $CD45^+$ populations from tumors were purified by FACS sorting. We performed single-cell 5′
850 gene expression profiling on the single-cell suspension using the Chromium Single Cell V(D)J
851 Solution from 10x Genomics according to the manufacturer's instructions. Cell-barcoded 5′ gene
852 expression libraries were sequenced on an Illumina NovaSeq6000 sequencer with pair-end reads.
853

854 *Gene expression UMI counts matrix generation*

855 The sequencing data were primarily analyzed by the 10× cellranger pipeline (v3.0.2) in two
856 steps. In the first step, cellranger mkfastq demultiplexed samples and generated fastq files; and in
857 the second step, cellranger count aligned fastq files to the reference genome and extracted gene
858 expression UMI counts matrix. In order to measure both human and viral gene expression, we
859 built a custom reference genome by integrating the MVA virus genome into the 10× pre-built
860 mouse reference using cellranger mkref. The MVA virus genome was downloaded from NCBI.
861

862 *Single-cell RNA-seq data analysis*

863 All cells expressing <200 or >6,000 genes were removed as well as cells that contained >5%
864 mitochondrial counts. Samples were merged and normalized. The default parameters of Seurat
865 were used, unless mentioned otherwise. Briefly, 2,000 variable genes were identified for the
866 clustering of all cell types and principal component analysis (PCA) was applied to the dataset to
867 reduce dimensionality after regressing for the number of UMIs (counts). The top 12-15 most
868 informative principal components (PCs) were used for clustering and Uniform Manifold
869 Approximation and Projection for dimension reduction (UMAP). To characterize each cluster,
870 we applied both the *FindAllMarkers* and *FindMarkers* procedure in Seurat, which identified
871 markers using log fold changes (FC) of mean expression. To identify differentially expressed
872 genes between two groups of clusters, *FindMarkers* functions in Seurat and Enhanced Volcano R
873 package (v1.8.0) were used. For subsequent T cell analysis, we first extracted all the $CD3^+$ cells
874 from the original dataset and repeated the clustering procedures in the T cell subset.
875

876 *Gene set enrichment analysis (GSEA)*

877 The GSEA analysis was done and visualized using the *clusterProfiler* (v4.0.5) and *enrichplot*
878 (v1.12.3) packages, which uses predefined gene sets from the Molecular Signatures Database

879 (MSigDB v7.4) [63]. We used the hallmark gene sets collection for the present study. Genes were
880 ranked by the test statistic value obtained from differential expression analysis and the pre-
881 ranked version of the tool was used to identify significantly enriched biological pathways.
882
883 **Statistical analysis**
884 Two-tailed unpaired Student's t test was used for comparisons of two groups in the studies.
885 Survival data were analyzed by log-rank (Mantel-Cox) test. The p values deemed significant are
886 indicated in the figures as follows: *, $p < 0.05$; **, $p < 0.01$; ***, $p < 0.001$; ****, $p < 0.0001$.
887 The numbers of animals included in the study are discussed in each figure legend.
888
889 **Lead Contact**
890
891 Further information and requests for resources and reagents used in this study should be directed
892 to and will be fulfilled by the lead contact and the corresponding author, Liang Deng
893 (dengl@mskcc.org).
894
895
896 **Materials availability**
897
898 Materials generated in our laboratory are available upon request.
899
900 **Data and code availability**
901 The scRNA-seq data reported in this study will be deposited in the Gene Expression Omnibus
902 database (GEO) and will make it available to the public after the manuscript is accepted for a
903 publication after peer-review.
904
905
906 **Acknowledgements**
907 We thank the Flow Cytometry Core Facility at the Sloan Kettering Institute and Genomic
908 Resources Core Facility Weill Cornell Medical College. This work was supported by NIH grants
909 K-08 AI073736 (L.D.), R56AI095692 (L.D.), R03 AR068118 (L.D.), R01 CA56821 (J.D.W),
910 Cancer Research Institute Irvington Postdoctoral Fellowship (L.L.J), Society of Memorial Sloan
911 Kettering (MSK) research grant (L.D.), MSK Technology Development Fund (L.D.), Parker
912 Institute for Cancer Immunotherapy Career Development Award (L.D.), sponsored research
913 agreement from IMVAQ Therapeutics (L.D.). This work was supported in part by the Swim
914 across America (J.D.W., T.M.), Ludwig Institute for Cancer Research (J.D.W., T.M.), This

research was also funded in part through the NIH/NCI Cancer Center Support Grant P30 CA008748.

Author Contributions

Author contributions: G.M. and L.D. designed the constructs and G.M. generated rMVAΔE3L, MQ832, and MQ833. G.M. generated various knock-out tumor cell lines in this study using CRISPR-cas9. G.M. and L.D. established the B2m$^{-/-}$ tumor model. S.L. and L.D. were involved in all aspect of this study, including designing and performing experiments, and data analyses and interpretation. and manuscript writing. S.L. performed scRNA-seq analyses with bioinformatics assistance from T.L. and A.T. from Genomic Resources Core Facility. N.Y. and Y.W. discovered WR199 as an inhibitor of cGAS and established the myeloid cell panel and T cell panel for flow cytometry. Y.W., S.B.T. and Y.Q.W, assisted some experiments. J.W., W.Y. J.C. assisted with construct designs and viral engineering. S.B.T produced most of the MQ833 for this study. L.L.J. produced anti-CSF1 antibody. D.H.C provided assistance on neutrophil-related study. J.D.W., T.M, M.O.L. and J.Z.X. assisted in some experimental design, data interpretation, and manuscript preparation. All authors are involved in manuscript preparation. L.D. provided overall supervision of the study.

Competing interests

Memorial Sloan Kettering Cancer Center filed a patent application for the use of recombinant MVA as monotherapy or in combination with immune checkpoint blockade for solid tumors. L.D., J.D.W., T.M., N.Y. Y.W. G.M. are authors on the patent, which has been licensed to IMVAQ Therapeutics. L.D., J.D.W., T.M., W.Y., J.C. and N.Y. are co-founders of IMVAQ Therapeutics. T.M. is a consultant of Immunos Therapeutics and Pfizer. He has research support from Bristol Myers Squibb; Surface Oncology; Kyn Therapeutics; Infinity Pharmaceuticals, Inc.; Peregrine Pharmaceuticals, Inc.; Adaptive Biotechnologies; Leap Therapeutics, Inc.; and Aprea. He has patents on applications related to work on oncolytic viral therapy, alpha virus-based vaccine, neoantigen modeling, CD40, GITR, OX40, PD-1, and CTLA-4. J.D.W. is a consultant for Adaptive Biotech, Advaxis, Am-gen, Apricity, Array BioPharma, Ascentage Pharma, Astellas, Bayer, Beigene, Bristol Myers Squibb, Celgene, Chugai, Elucida, Eli Lilly, F Star, Genentech, Imvaq, Janssen, Kleo Pharma, Linnaeus, MedImmune, Merck, Neon Therapeutics,

946 Ono, Polaris Pharma, Polynoma, Psioxus, Puretech, Recepta, Trieza, Sellas Life Sciences,
947 Serametrix, Surface Oncology, and Syndax. Research support: Bristol Myers Squibb,
948 Medimmune, Merck Pharmaceuticals, and Genentech. Equity: Potenza Therapeutics, Tizona
949 Pharmaceuticals, Adaptive Biotechnologies, Elucida, Imvaq, Beigene, Trieza, and Linnaeus.
950 Honorarium: Esanex. Patents: xenogeneic DNA vaccines, alphavirus replicon particles ex-
951 pressing TRP2, MDSC assay, Newcastle disease viruses for cancer therapy, genomic signature to
952 identify responders to ipilimumab in melanoma, engineered vaccinia viruses for cancer
953 immunotherapy, anti-CD40 agonist mono-clonal antibody (mAb) fused to monophosphoryl lipid
954 A (MPL) for cancer therapy, CAR T cells targeting differentiation antigens as means to treat
955 cancer, anti-PD-1 antibody, anti-CTLA-4 antibodies, and anti-GITR antibodies and methods of
956 use thereof.
957

References

958 1. Binnewies, M. *et al.* Understanding the tumor immune microenvironment (TIME) for
959 effective therapy. *Nat Med* **24**, 541-550 (2018).
960
961 2. Tcyganov, E., Mastio, J., Chen, E. & Gabrilovich, D.I. Plasticity of myeloid-derived
962 suppressor cells in cancer. *Curr Opin Immunol* **51**, 76-82 (2018).
963
964 3. Gajewski, T.F., Schreiber, H. & Fu, Y.X. Innate and adaptive immune cells in the tumor
965 microenvironment. *Nat Immunol* **14**, 1014-1022 (2013).
966
967 4. Kim, T.K., Vandsemb, E.N., Herbst, R.S. & Chen, L. Adaptive immune resistance at the
968 tumour site: mechanisms and therapeutic opportunities. *Nat Rev Drug Discov* **21**, 529-
969 540 (2022).
970
971 5. Kraehenbuehl, L., Weng, C.H., Eghbali, S., Wolchok, J.D. & Merghoub, T. Enhancing
972 immunotherapy in cancer by targeting emerging immunomodulatory pathways. *Nat Rev*
973 *Clin Oncol* **19**, 37-50 (2022).
974
975 6. Ribas, A. & Wolchok, J.D. Cancer immunotherapy using checkpoint blockade. *Science*
976 **359**, 1350-1355 (2018).
977
978 7. Zappasodi, R., Merghoub, T. & Wolchok, J.D. Emerging Concepts for Immune Checkpoint
979 Blockade-Based Combination Therapies. *Cancer Cell* **34**, 690 (2018).
980
981 8. Wang, Y., Johnson, K.C.C., Gatti-Mays, M.E. & Li, Z. Emerging strategies in targeting
982 tumor-resident myeloid cells for cancer immunotherapy. *J Hematol Oncol* **15**, 118
983 (2022).
984
985 9. Jaillon, S. *et al.* Neutrophil diversity and plasticity in tumour progression and therapy.
986 *Nat Rev Cancer* **20**, 485-503 (2020).
987
988 10. Bommareddy, P.K., Shettigar, M. & Kaufman, H.L. Integrating oncolytic viruses in
989 combination cancer immunotherapy. *Nat Rev Immunol* **18**, 498-513 (2018).
990
991 11. Melcher, A., Harrington, K. & Vile, R. Oncolytic virotherapy as immunotherapy. *Science*
992 **374**, 1325-1326 (2021).
993
994 12. Russell, S.J. & Barber, G.N. Oncolytic Viruses as Antigen-Agnostic Cancer Vaccines.
995 *Cancer Cell* **33**, 599-605 (2018).
996
997 13. Kaufman, H.L., Kohlhapp, F.J. & Zloza, A. Oncolytic viruses: a new class of
998 immunotherapy drugs. *Nat Rev Drug Discov* **14**, 642-662 (2015).
999

1000 14. Davola, M.E. & Mossman, K.L. Oncolytic viruses: how "lytic" must they be for
1001 therapeutic efficacy? *Oncoimmunology* **8**, e1581528 (2019).
1002
1003 15. Brown, M.C. *et al.* Viral infection of cells within the tumor microenvironment mediates
1004 antitumor immunotherapy via selective TBK1-IRF3 signaling. *Nat Commun* **12**, 1858
1005 (2021).
1006
1007 16. Wang, W. *et al.* Elucidating mechanisms of antitumor immunity mediated by live
1008 oncolytic vaccinia and heat-inactivated vaccinia. *J Immunother Cancer* **9** (2021).
1009
1010 17. Dai, P. *et al.* Intratumoral delivery of inactivated modified vaccinia virus Ankara (iMVA)
1011 induces systemic antitumor immunity via STING and Batf3-dependent dendritic cells. *Sci*
1012 *Immunol* **2** (2017).
1013
1014 18. Stickl, H. & Hochstein-Mintzel, V. [Intracutaneous smallpox vaccination with a weak
1015 pathogenic vaccinia virus ("MVA virus")]. *Munch Med Wochenschr* **113**, 1149-1153
1016 (1971).
1017
1018 19. Antoine, G., Scheiflinger, F., Dorner, F. & Falkner, F.G. The complete genomic sequence
1019 of the modified vaccinia Ankara strain: comparison with other orthopoxviruses. *Virology*
1020 **244**, 365-396 (1998).
1021
1022 20. Pittman, P.R. *et al.* Phase 3 Efficacy Trial of Modified Vaccinia Ankara as a Vaccine
1023 against Smallpox. *N Engl J Med* **381**, 1897-1908 (2019).
1024
1025 21. Gilbert, S.C. Clinical development of Modified Vaccinia virus Ankara vaccines. *Vaccine*
1026 **31**, 4241-4246 (2013).
1027
1028 22. Volz, A. & Sutter, G. Modified Vaccinia Virus Ankara: History, Value in Basic Research,
1029 and Current Perspectives for Vaccine Development. *Adv Virus Res* **97**, 187-243 (2017).
1030
1031 23. Overton, E.T. *et al.* Safety and Immunogenicity of Modified Vaccinia Ankara-Bavarian
1032 Nordic Smallpox Vaccine in Vaccinia-Naive and Experienced Human Immunodeficiency
1033 Virus-Infected Individuals: An Open-Label, Controlled Clinical Phase II Trial. *Open Forum*
1034 *Infect Dis* **2**, ofv040 (2015).
1035
1036 24. Dai, P. *et al.* Modified vaccinia virus Ankara triggers type I IFN production in murine
1037 conventional dendritic cells via a cGAS/STING-mediated cytosolic DNA-sensing pathway.
1038 *PLoS Pathog* **10**, e1003989 (2014).
1039
1040 25. Yang, N. *et al.* Intratumoral delivery of engineered recombinant modified vaccinia virus
1041 Ankara expressing Flt3L and OX40L generates potent antitumor immunity through
1042 activating the cGAS/STING pathway and depleting tumor-infiltrating regulatory T cells.
1043 *bioRxiv*, 2021.2010.2031.466698 (2021).

1044
1045 26. Yang, N. *et al.* Vaccinia E5 is a major inhibitor of the DNA sensor cGAS. *bioRxiv*,
1046 2021.2010.2025.465197 (2021).
1047
1048 27. Liu, K. & Nussenzweig, M.C. Origin and development of dendritic cells. *Immunol Rev* **234**,
1049 45-54 (2010).
1050
1051 28. Croft, M. The role of TNF superfamily members in T-cell function and diseases. *Nat Rev*
1052 *Immunol* **9**, 271-285 (2009).
1053
1054 29. Deng, L. *et al.* Vaccinia virus subverts a mitochondrial antiviral signaling protein-
1055 dependent innate immune response in keratinocytes through its double-stranded RNA
1056 binding protein, E3. *J Virol* **82**, 10735-10746 (2008).
1057
1058 30. Sperling, K.M., Schwantes, A., Schnierle, B.S. & Sutter, G. The highly conserved
1059 orthopoxvirus 68k ankyrin-like protein is part of a cellular SCF ubiquitin ligase complex.
1060 *Virology* **374**, 234-239 (2008).
1061
1062 31. Liu, B. *et al.* Identification of Poxvirus Genome Uncoating and DNA Replication Factors
1063 with Mutually Redundant Roles. *J Virol* **92** (2018).
1064
1065 32. Kobayashi, M. *et al.* Identification and purification of natural killer cell stimulatory factor
1066 (NKSF), a cytokine with multiple biologic effects on human lymphocytes. *J Exp Med* **170**,
1067 827-845 (1989).
1068
1069 33. Trinchieri, G. Interleukin-12 and the regulation of innate resistance and adaptive
1070 immunity. *Nat Rev Immunol* **3**, 133-146 (2003).
1071
1072 34. Ge, Y. *et al.* Oncolytic vaccinia virus delivering tethered IL-12 enhances antitumor effects
1073 with improved safety. *J Immunother Cancer* **8** (2020).
1074
1075 35. Nakao, S. *et al.* Intratumoral expression of IL-7 and IL-12 using an oncolytic virus
1076 increases systemic sensitivity to immune checkpoint blockade. *Sci Transl Med* **12** (2020).
1077
1078 36. Saha, D., Martuza, R.L. & Rabkin, S.D. Macrophage Polarization Contributes to
1079 Glioblastoma Eradication by Combination Immunovirotherapy and Immune Checkpoint
1080 Blockade. *Cancer Cell* **32**, 253-267 e255 (2017).
1081
1082 37. Wyatt, L.S., Shors, S.T., Murphy, B.R. & Moss, B. Development of a replication-deficient
1083 recombinant vaccinia virus vaccine effective against parainfluenza virus 3 infection in an
1084 animal model. *Vaccine* **14**, 1451-1458 (1996).
1085
1086 38. Herrera, F.G. *et al.* Low-Dose Radiotherapy Reverses Tumor Immune Desertification and
1087 Resistance to Immunotherapy. *Cancer Discov* **12**, 108-133 (2022).

1088
1089 39. DeNardo, D.G. *et al.* Leukocyte complexity predicts breast cancer survival and
1090 functionally regulates response to chemotherapy. *Cancer Discov* **1**, 54-67 (2011).
1091
1092 40. Basudhar, D. *et al.* Coexpression of NOS2 and COX2 accelerates tumor growth and
1093 reduces survival in estrogen receptor-negative breast cancer. *Proc Natl Acad Sci U S A*
1094 **114**, 13030-13035 (2017).
1095
1096 41. Xu, W., Liu, L.Z., Loizidou, M., Ahmed, M. & Charles, I.G. The role of nitric oxide in
1097 cancer. *Cell Res* **12**, 311-320 (2002).
1098
1099 42. Sharma, P., Hu-Lieskovan, S., Wargo, J.A. & Ribas, A. Primary, Adaptive, and Acquired
1100 Resistance to Cancer Immunotherapy. *Cell* **168**, 707-723 (2017).
1101
1102 43. Zaretsky, J.M. *et al.* Mutations Associated with Acquired Resistance to PD-1 Blockade in
1103 Melanoma. *N Engl J Med* **375**, 819-829 (2016).
1104
1105 44. Sade-Feldman, M. *et al.* Resistance to checkpoint blockade therapy through inactivation
1106 of antigen presentation. *Nat Commun* **8**, 1136 (2017).
1107
1108 45. Motzer, R.J. *et al.* Phase I trial of subcutaneous recombinant human interleukin-12 in
1109 patients with advanced renal cell carcinoma. *Clin Cancer Res* **4**, 1183-1191 (1998).
1110
1111 46. Leonard, J.P. *et al.* Effects of single-dose interleukin-12 exposure on interleukin-12-
1112 associated toxicity and interferon-gamma production. *Blood* **90**, 2541-2548 (1997).
1113
1114 47. Zhou, X. *et al.* Differentiation and persistence of memory CD8(+) T cells depend on T cell
1115 factor 1. *Immunity* **33**, 229-240 (2010).
1116
1117 48. Jeannet, G. *et al.* Essential role of the Wnt pathway effector Tcf-1 for the establishment
1118 of functional CD8 T cell memory. *Proc Natl Acad Sci U S A* **107**, 9777-9782 (2010).
1119
1120 49. Siddiqui, I. *et al.* Intratumoral Tcf1(+)PD-1(+)CD8(+) T Cells with Stem-like Properties
1121 Promote Tumor Control in Response to Vaccination and Checkpoint Blockade
1122 Immunotherapy. *Immunity* **50**, 195-211 e110 (2019).
1123
1124 50. Silvestre-Roig, C., Fridlender, Z.G., Glogauer, M. & Scapini, P. Neutrophil Diversity in
1125 Health and Disease. *Trends Immunol* **40**, 565-583 (2019).
1126
1127 51. Hedrick, C.C. & Malanchi, I. Neutrophils in cancer: heterogeneous and multifaceted. *Nat*
1128 *Rev Immunol* **22**, 173-187 (2022).
1129
1130 52. Carnevale, S., Ghasemi, S., Rigatelli, A. & Jaillon, S. The complexity of neutrophils in
1131 health and disease: Focus on cancer. *Semin Immunol* **48**, 101409 (2020).

53. Sagiv, J.Y. *et al.* Phenotypic diversity and plasticity in circulating neutrophil subpopulations in cancer. *Cell Rep* **10**, 562-573 (2015).

54. Giese, M.A., Hind, L.E. & Huttenlocher, A. Neutrophil plasticity in the tumor microenvironment. *Blood* **133**, 2159-2167 (2019).

55. Wculek, S.K. & Malanchi, I. Neutrophils support lung colonization of metastasis-initiating breast cancer cells. *Nature* **528**, 413-417 (2015).

56. Coffelt, S.B. *et al.* IL-17-producing gammadelta T cells and neutrophils conspire to promote breast cancer metastasis. *Nature* **522**, 345-348 (2015).

57. Fridlender, Z.G. *et al.* Polarization of tumor-associated neutrophil phenotype by TGF-beta: "N1" versus "N2" TAN. *Cancer Cell* **16**, 183-194 (2009).

58. Takeshima, T. *et al.* Key role for neutrophils in radiation-induced antitumor immune responses: Potentiation with G-CSF. *Proc Natl Acad Sci U S A* **113**, 11300-11305 (2016).

59. Gitlin, L. *et al.* Essential role of mda-5 in type I IFN responses to polyriboinosinic:polyribocytidylic acid and encephalomyocarditis picornavirus. *Proc Natl Acad Sci U S A* **103**, 8459-8464 (2006).

60. Yang, N. *et al.* Lung type II alveolar epithelial cells collaborate with CCR2(+) inflammatory monocytes in host defense against poxvirus infection. *Nat Commun* **13**, 1671 (2022).

61. Lokeshwar, B.L. & Lin, H.S. Development and characterization of monoclonal antibodies to murine macrophage colony-stimulating factor. *J Immunol* **141**, 483-488 (1988).

62. Cenci, S., Weitzmann, M.N., Gentile, M.A., Aisa, M.C. & Pacifici, R. M-CSF neutralization and egr-1 deficiency prevent ovariectomy-induced bone loss. *J Clin Invest* **105**, 1279-1287 (2000).

63. Subramanian, A. *et al.* Gene set enrichment analysis: a knowledge-based approach for interpreting genome-wide expression profiles. *Proc Natl Acad Sci U S A* **102**, 15545-15550 (2005).

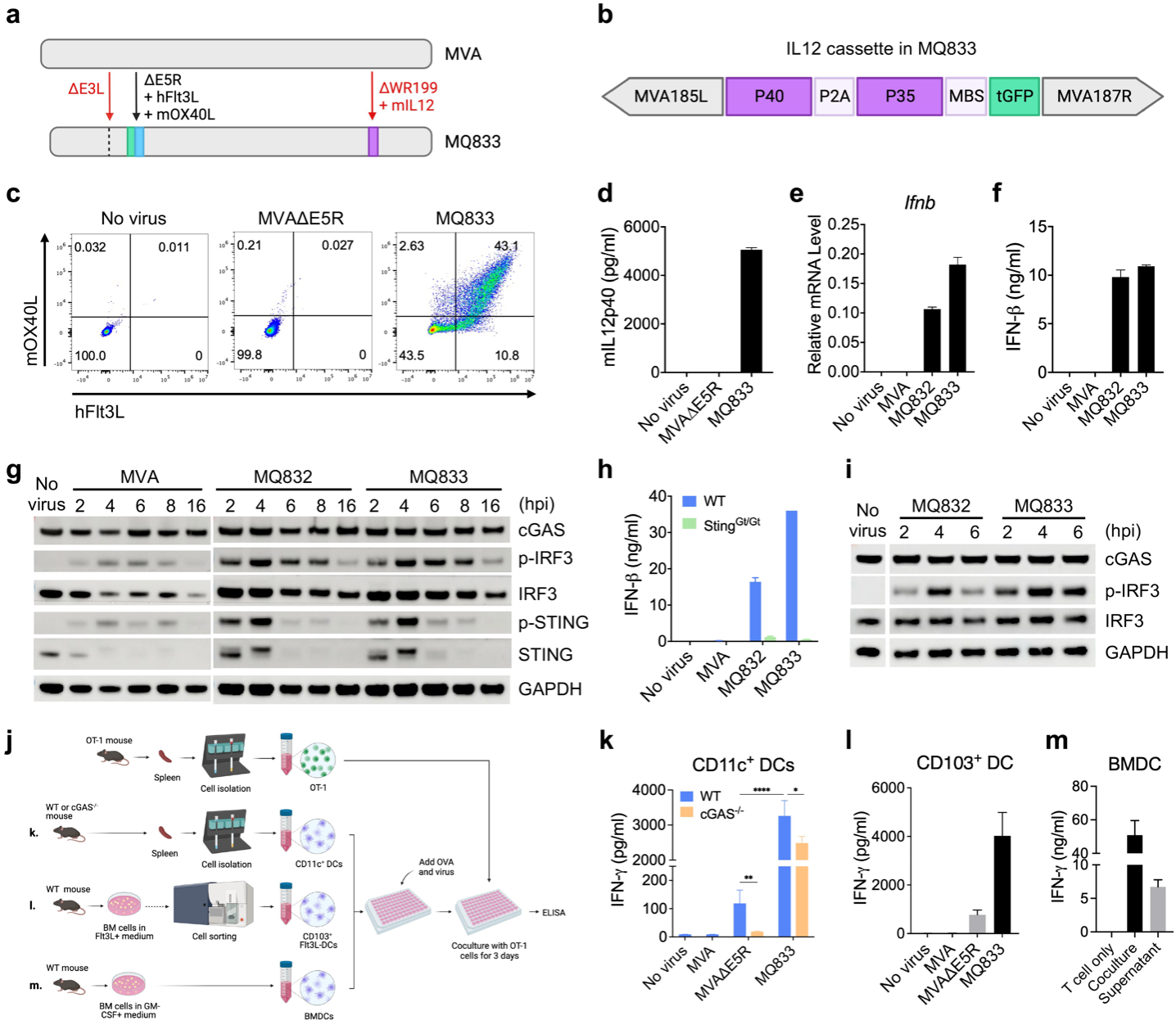
a
MVA
ΔE3L
ΔE5R
+ hFlt3L
+ mOX40L
ΔWR199
+ mIL12
MQ833
b
IL12 cassette in MQ833
MVA185L
P40
P2A
P35
MBS
tGFP
MVA187R
c
No virus
MVAΔE5R
MQ833
mOX40L
hFlt3L
0.032
0.011
100.0
0
0.21
0.027
99.8
0
2.63
43.1
43.5
10.8
d
mIL12p40 (pg/ml)
No virus
MVAΔE5R
MQ833
e
Ifnb
Relative mRNA Level
No virus
MVA
MQ832
MQ833
f
IFN-β (ng/ml)
No virus
MVA
MQ832
MQ833
g
No virus
MVA
MQ832
MQ833
(hpi)
cGAS
p-IRF3
IRF3
p-STING
STING
GAPDH
h
WT
Sting^Gt/Gt
IFN-β (ng/ml)
No virus
MVA
MQ832
MQ833
i
No virus
MQ832
MQ833
(hpi)
cGAS
p-IRF3
IRF3
GAPDH
j
OT-1 mouse
Spleen
Cell isolation
OT-1
WT or cGAS-/- mouse
k.
CD11c+ DCs
WT mouse
l.
BM cells in Flt3L+ medium
Cell sorting
CD103+ Flt3L-DCs
WT mouse
m.
BM cells in GM-CSF+ medium
BMDCs
Add OVA and virus
Coculture with OT-1 cells for 3 days
ELISA
k
CD11c+ DCs
WT
cGAS-/-
IFN-γ (pg/ml)
No virus
MVA
MVAΔE5R
MQ833
l
CD103+ DC
IFN-γ (pg/ml)
No virus
MVA
MVAΔE5R
MQ833
m
BMDC
IFN-γ (ng/ml)
T cell only
Coculture
Supernatant

1172 **Fig. 1 | MQ833 infection of tumor and immune cells activates cGAS/STING mediated**
1173 **dsDNA sensing pathway and promotes IFN production. a**, Diagram of MQ833 design. **b**,
1174 Diagram of the IL12 cassette. **c**,**d**, B16-F10 cells were infected by MVAΔE5R or MQ833 at a
1175 MOI of 10. Cells and supernatant were collected at 16 hours post infection (hpi). **c**, Flow
1176 cytometric analysis of mOX40L and hFlt3L transgene expression. **d**, ELISA test for mIL12p40.
1177 **e**,**f**, B16-F10 cells were infected with indicated viruses at a MOI of 10, and cells and supernatant
1178 were collected 16 hpi. **e**, RT-PCR for *Ifnb* gene expression. **f**, ELISA test for IFN-β. **g**, Western
1179 blot for indicated protein and phosphorylated proteins in the cGAS-STING pathway. B16-F10
1180 cells were infected with indicated viruses at a MOI of 10, and cells were collected at 2, 4, 6, 8,
1181 16 hours post infection (hpi). **h**,**i**, BMDCs from WT or *Sting*$^{Gt/Gt}$ mice were infected with
1182 indicated viruses at a MOI of 10. Cells were lysed and collected for western blot at indicated
1183 time points post infection. Supernatants were collected at 16 hours post infection. **h**, ELISA for
1184 IFN-γ. **i**, Western blot for cGAS, p-IRF3, IRF3, and GAPDH. **j**, Schematic diagram for DC and
1185 T cell coculture experiment. **k-m,** ELISA for IFN-γ level in supernatants from the coculture
1186 system. **k**, CD11c^{+} DCs were isolated from the spleens of WT C57BL/6J or cGAS$^{-/-}$ mice, pulsed
1187 with OVA, and infected with different viruses. OT-1 cells isolated from OT-1 mice were then
1188 added to the DCs and cocultured for 3 days. Supernatants were collected and IFN-γ level was
1189 measured by ELISA. Data are means ± SD (*n=3; *P < 0.05, ****P < 0.0001, t test*). **l**, CD103^{+}
1190 DCs were sorted from Flt3L+ DCs and and subsequently pulsed with OVA and infected with
1191 different viruses. OT-1 cells isolated from OT-1 mice were then added to the DCs and co-
1192 cultured for 3 days. Supernatants were collected and IFN-γ level was measured by ELISA. **m**,
1193 BMDCs were pulsed with OVA and infected with MQ833. OT-1 cells were either cocultured
1194 with pulsed and infected BMDCs or cultured in medium from the infected BMDC for 3 days.

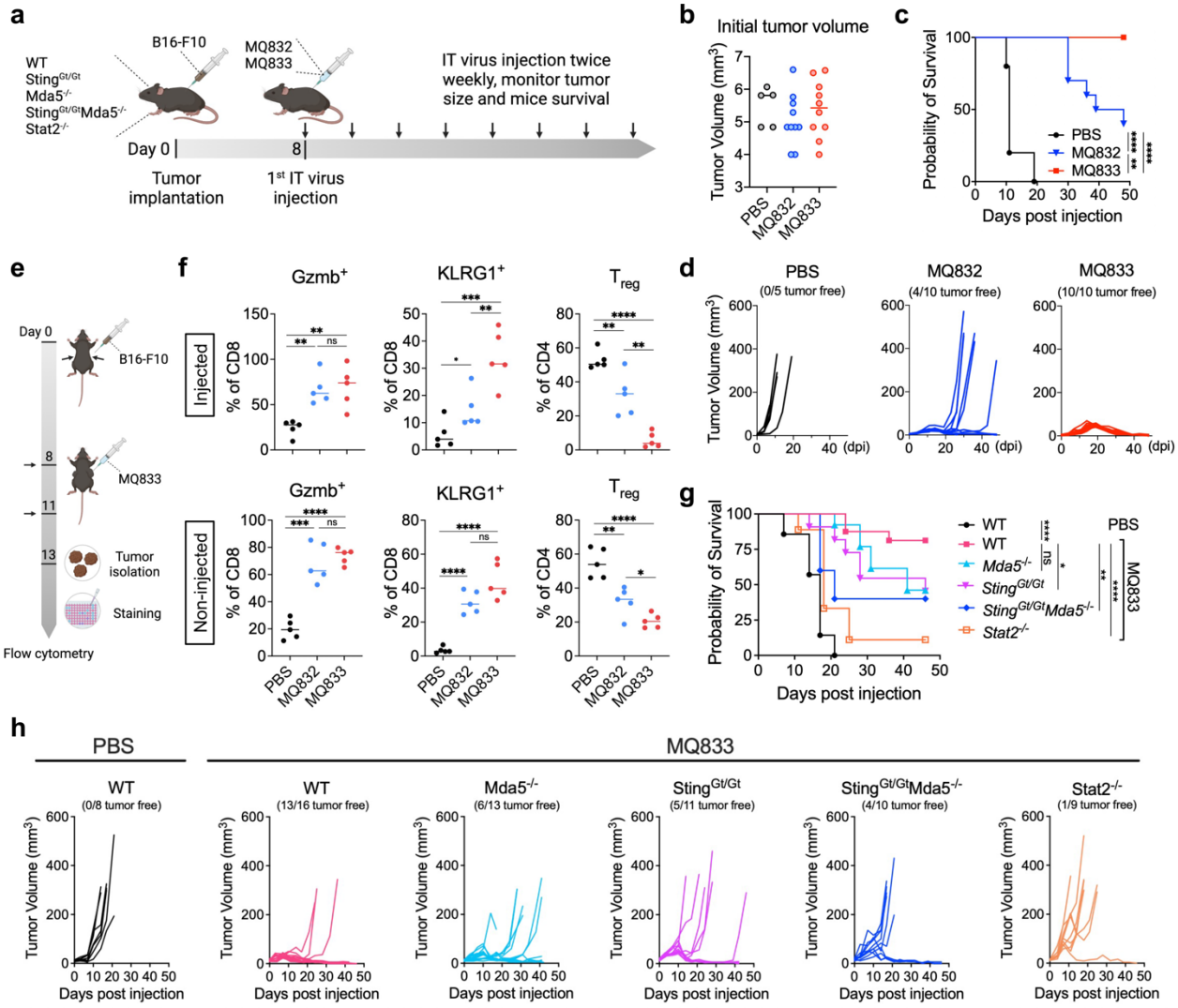
a
WT
Sting$^{Gt/Gt}$
Mda5$^{-/-}$
Sting$^{Gt/Gt}$Mda5$^{-/-}$
Stat2$^{-/-}$
B16-F10
MQ832
MQ833
IT virus injection twice weekly, monitor tumor size and mice survival
Day 0
8
Tumor implantation
1st IT virus injection
b
Initial tumor volume
Tumor Volume (mm^3)
PBS
MQ832
MQ833
c
Probability of Survival
Days post injection
PBS
MQ832
MQ833
e
Day 0
B16-F10
8
MQ833
11
13
Tumor isolation
Staining
Flow cytometry
f
Gzmb$^+$
KLRG1$^+$
T$_{reg}$
Injected
Non-injected
% of CD8
% of CD4
PBS
MQ832
MQ833
d
PBS
(0/5 tumor free)
MQ832
(4/10 tumor free)
MQ833
(10/10 tumor free)
Tumor Volume (mm^3)
(dpi)
g
Probability of Survival
Days post injection
WT
WT
Mda5$^{-/-}$
Sting$^{Gt/Gt}$
Sting$^{Gt/Gt}$Mda5$^{-/-}$
Stat2$^{-/-}$
PBS
MQ833
h
PBS
MQ833
WT
(0/8 tumor free)
WT
(13/16 tumor free)
Mda5$^{-/-}$
(6/13 tumor free)
Sting$^{Gt/Gt}$
(5/11 tumor free)
Sting$^{Gt/Gt}$Mda5$^{-/-}$
(4/10 tumor free)
Stat2$^{-/-}$
(1/9 tumor free)
Tumor Volume (mm^3)
Days post injection

1195 **Fig.2 | Intratumoral (IT) delivery of MQ833 generates an 80-100% cure in B16-F10**
1196 **melanoma model in a STING-MDA5-STAT2-dependent manner**
1197 **a**, 5 x10^5 of B16-F10 cells were intradermally implanted into the right flank of WT C57BL/6J
1198 mice (**b-e**), Mda5$^{-/-}$, Sting$^{Gt/Gt}$, Mda5$^{-/-}$ Sting$^{Gt/Gt}$, or Stat2$^{-/-}$ mice (**f,g**). Intratumoral virus
1199 treatments were given twice a week once the tumors were established. Tumor size and mice
1200 survival were monitored. **b,** Kaplan-Meier survival curve of B16-F10 tumor bearing mice treated
1201 with MQ833 virus. PBS was used as a control. Survival data were analyzed by log-rank (Mantel-
1202 Cox) test (n=5-10, ***P<0.01, ****P < 0.0001*). **c,** Initial tumor volume for each group. **d,**
1203 Tumor volumes of mice injected with MQ832, MQ833 or PBS over days post treatment. **e**,
1204 Schematic diagram of flow cytometric analysis of tumor infiltrating lymphocytes. WT C57BL/6J
1205 mice were implanted with B16-F10 cells on the right (5 x10^5) and left (2.5 x10^5) flanks. Once the
1206 tumors were established, 2 doses of 4 x10^7 PFU of MQ833 were intratumorally delivered to the
1207 right flanks twice, 3 days apart. Injected and non-injected tumors were harvested at day 2 post
1208 the second injection and then stained and analyzed by flow cytometry. **f**, Percentages of
1209 CD8$^+$Granzyme B$^+$, KLRG1$^+$CD8$^+$, and CD4$^+$Foxp3$^+$ T cells in the injected and non-injected
1210 tumors in different treatment groups. Data are means ± SD (*n=5; *P<0.05, **P<0.01,*
1211 ****P<0.001, ****P < 0.0001, t test*). **g**, Kaplan-Meier survival curve of B16-F10 tumor bearing
1212 mice treated with MQ833 virus. PBS was used as a control. Survival data were analyzed by log-
1213 rank (Mantel-Cox) test (n=8-16, ***P<0.01, ****P < 0.0001*). **h**, Tumor volume curves in
1214 different groups over days post treatment.

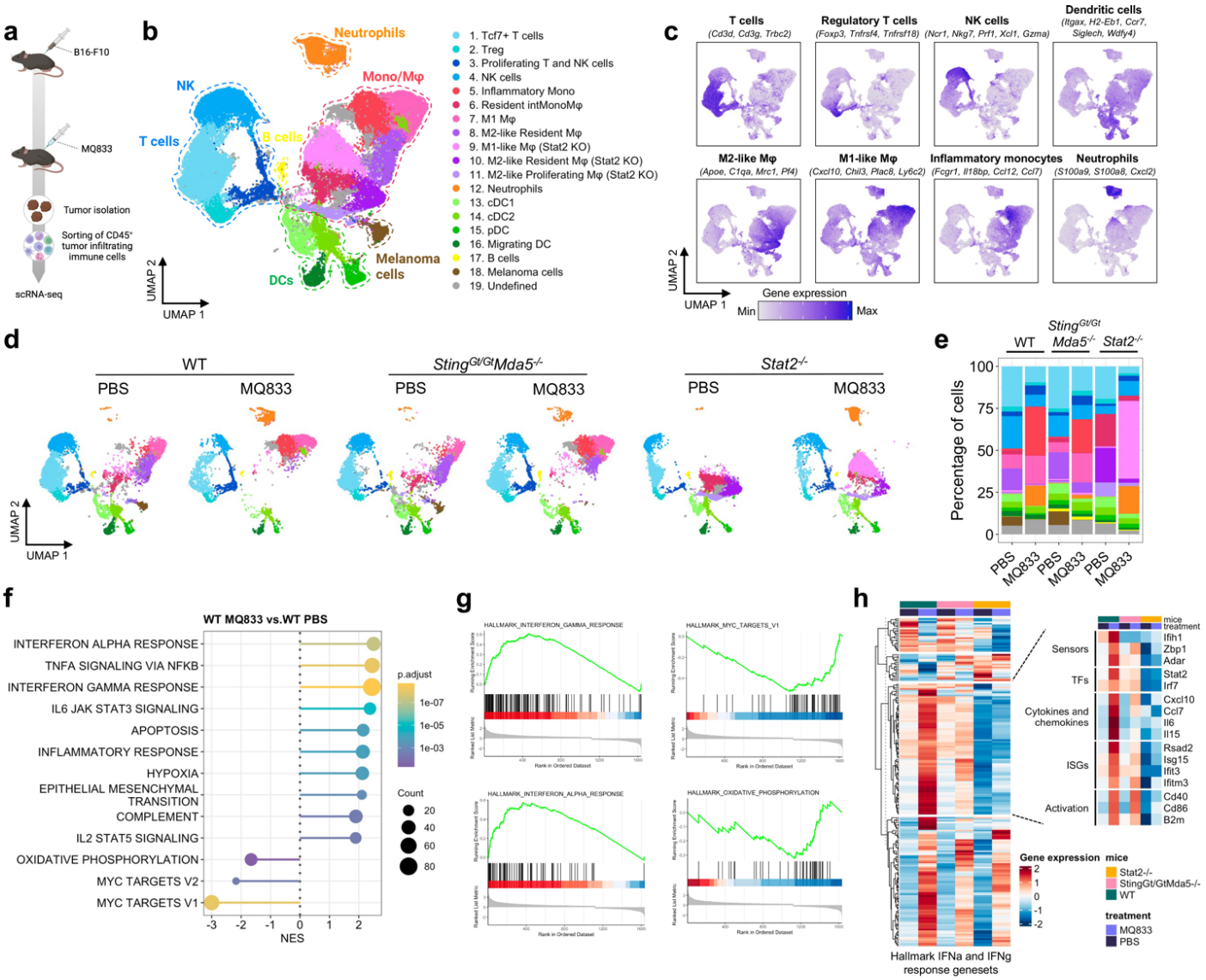
a
B16-F10
MQ833
Tumor isolation
Sorting of CD45+ tumor infiltrating immune cells
scRNA-seq
b
Neutrophils
Mono/Mφ
NK
T cells
B cells
DCs
Melanoma cells
UMAP 2
UMAP 1
1. Tcf7+ T cells
2. Treg
3. Proliferating T and NK cells
4. NK cells
5. Inflammatory Mono
6. Resident intMonoMφ
7. M1 Mφ
8. M2-like Resident Mφ
9. M1-like Mφ (Stat2 KO)
10. M2-like Resident Mφ (Stat2 KO)
11. M2-like Proliferating Mφ (Stat2 KO)
12. Neutrophils
13. cDC1
14. cDC2
15. pDC
16. Migrating DC
17. B cells
18. Melanoma cells
19. Undefined
c
T cells (Cd3d, Cd3g, Trbc2)
Regulatory T cells (Foxp3, Tnfrsf4, Tnfrsf18)
NK cells (Ncr1, Nkg7, Prf1, Xcl1, Gzma)
Dendritic cells (Itgax, H2-Eb1, Ccr7, Siglech, Wdfy4)
M2-like Mφ (Apoe, C1qa, Mrc1, Pf4)
M1-like Mφ (Cxcl10, Chil3, Plac8, Ly6c2)
Inflammatory monocytes (Fcgr1, Il18bp, Ccl12, Ccl7)
Neutrophils (S100a9, S100a8, Cxcl2)
Gene expression
Min
Max
d
WT
PBS
MQ833
StingGt/GtMda5-/-
Stat2-/-
e
Percentage of cells
f
WT MQ833 vs.WT PBS
INTERFERON ALPHA RESPONSE
TNFA SIGNALING VIA NFKB
INTERFERON GAMMA RESPONSE
IL6 JAK STAT3 SIGNALING
APOPTOSIS
INFLAMMATORY RESPONSE
HYPOXIA
EPITHELIAL MESENCHYMAL TRANSITION
COMPLEMENT
IL2 STAT5 SIGNALING
OXIDATIVE PHOSPHORYLATION
MYC TARGETS V2
MYC TARGETS V1
NES
p.adjust
Count
g
HALLMARK_INTERFERON_GAMMA_RESPONSE
HALLMARK_MYC_TARGETS_V1
HALLMARK_INTERFERON_ALPHA_RESPONSE
HALLMARK_OXIDATIVE_PHOSPHORYLATION
h
Sensors
TFs
Cytokines and chemokines
ISGs
Activation
Ifih1
Zbp1
Adar
Stat2
Irf7
Cxcl10
Ccl7
Il6
Il15
Rsad2
Isg15
Ifit3
Ifitm3
Cd40
Cd86
B2m
Gene expression
mice
Stat2-/-
StingGt/GtMda5-/-
WT
treatment
MQ833
PBS
Hallmark IFNa and IFNg response genesets
i
WT MQ833 vs. WT PBS
Neutrophils
Down in MQ833
Up in MQ833
non-significant
Fcer1a
Ms4a2
B2m
Il4
Isg15
Ifit3
Gbp2
Clec4d
Irf7
Cxcl10
Cd274
Cd14
Ifi27l2a
Log2 fold change
WT MQ833 vs. DKO MQ833
Igkc
H2-Q6
Ifih1
H2-Ab1
Ifi209
Ifi213
Spp1
Ifitm1
Ifit1
WT MQ833 vs. STAT2 KO MQ833
Up in WT
Down in WT
Ifi27l2a
Ifit3
Isg15
Irf7
B2m
Cxcl10
Il1rn
Fcgr1
Stat2
j
Anti-tumor
Pro-tumor
Fas
Il12a
Ifng
Nos2
Cxcl1
Cxcl10
Arg1
Mmp9
Elane
Il1b

1215 **Fig. 3 | IT MQ833 injection reprograms the tumor-infiltrated myeloid cells. a,** Schematic
1216 diagram of the experimental schedule. $5x10^5$ of B16-F10 cells were intradermally implanted into
1217 the right flank of WT C57BL/6J mice, *Mda5*$^{-/-}$ *Sting*$^{Gt/Gt}$, or *Stat2*$^{-/-}$ mice. One IT MQ833
1218 injection was given once the tumors were established. Tumors were collected and processed into
1219 single cell suspension, and $CD45^+$ cells were sorted and scRNA-seq analyses were performed. **b,**
1220 UMAP display of sorted $CD45^+$ cells from 6 samples combined following 10X Genomics
1221 scRNA-seq workflow (n = 47020 cells). **c,** Expression plots of 8 main cell types using their top
1222 marker genes. **d,** UMAP plots of cell clusters separated by sample. **e,** Stacked bar plot showing
1223 the percentage of each cluster across different samples. **f,** Dot plot for the top enriched and
1224 suppressed gene sets from the Molecular Signature Database (MSigDB) Hallmark immunologic
1225 signature gene sets in WT MQ833 versus WT PBS. **g,** Gene set enrichment analysis (GSEA) for
1226 individual pathways from the representative enriched and suppressed gene sets in WT MQ833
1227 sample compared with WT PBS. **h**, Heatmaps of the average expression of genes in the hallmark
1228 IFNα and IFNγ response gene sets. Selected genes of interest are labeled in the right panel. **i,**
1229 Volcano plots of differentially expressed genes in neutrophil clusters between indicated samples.
1230 Important genes are highlighted. **j,** Heatmaps of the average expression of representative genes
1231 from the hallmark IFNα and IFNγ response gene sets (left panel) and marker genes for anti-
1232 tumor or pro-tumor neutrophils (right panel).

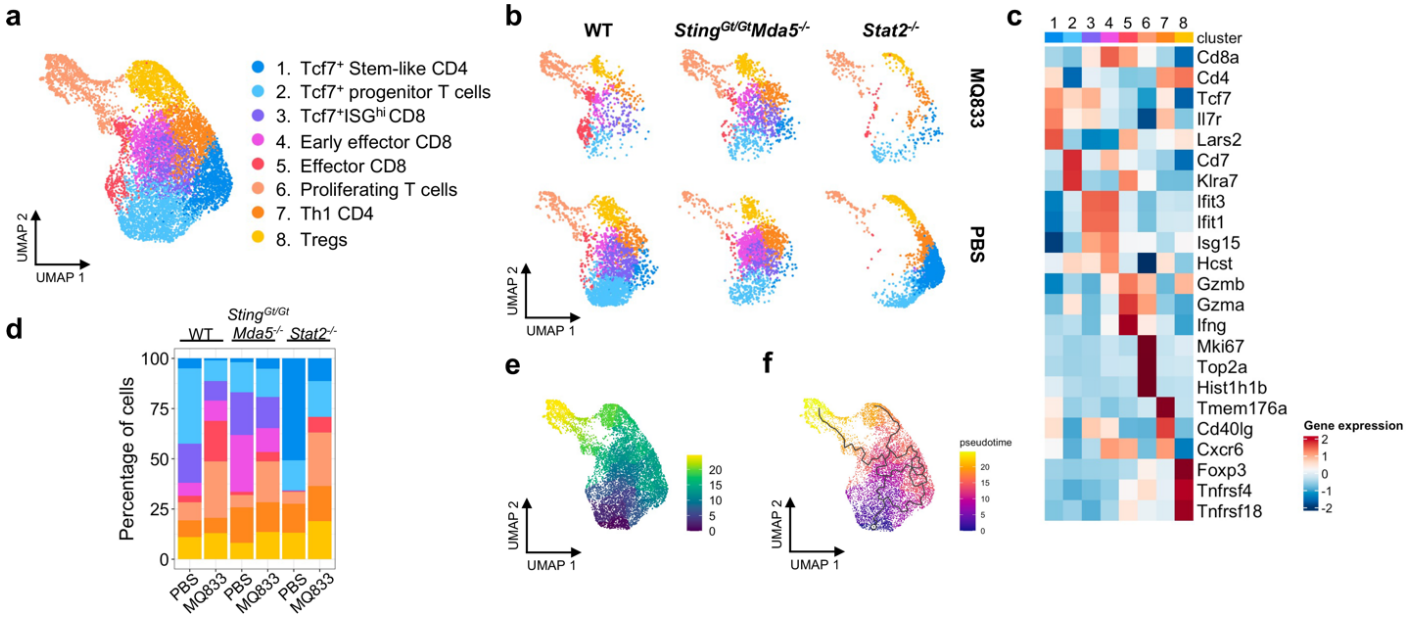
a
1. Tcf7+ Stem-like CD4
2. Tcf7+ progenitor T cells
3. Tcf7+ISGhi CD8
4. Early effector CD8
5. Effector CD8
6. Proliferating T cells
7. Th1 CD4
8. Tregs
UMAP 2
UMAP 1
b
WT
StingGt/GtMda5-/-
Stat2-/-
MQ833
PBS
UMAP 2
UMAP 1
c
1 2 3 4 5 6 7 8
cluster
Cd8a
Cd4
Tcf7
Il7r
Lars2
Cd7
Klra7
Ifit3
Ifit1
Isg15
Hcst
Gzmb
Gzma
Ifng
Mki67
Top2a
Hist1h1b
Tmem176a
Cd40lg
Cxcr6
Foxp3
Tnfrsf4
Tnfrsf18
Gene expression
2
1
0
-1
-2
d
StingGt/Gt
WT
Mda5-/-
Stat2-/-
Percentage of cells
100
75
50
25
0
PBS
MQ833
PBS
MQ833
PBS
MQ833
e
20
15
10
5
0
UMAP 2
UMAP 1
f
pseudotime
20
15
10
5
0
UMAP 2
UMAP 1

1233 **Fig. 4 | IT MQ833 injection reprograms the tumor-infiltrated T cells.** 5 x10^5 of B16-F10
1234 cells were intradermally implanted into the right flank of WT C57BL/6J mice, *Mda5*$^{-/-}$ *Sting*$^{Gt/Gt}$,
1235 or *Stat2*$^{-/-}$ mice. One dose of IT MQ833 injection was given once the tumors were established.
1236 Tumors were collected and processed into single cell suspension, and CD45$^+$ cells were sorting
1237 and sent for scRNA-seq. **a,** UMAP display of subclustered CD45$^+$CD3$^+$ cells from 6 samples
1238 combined following 10X Genomics scRNA-seq workflow (n = 9,540 cells). **b,** UMAP plots of
1239 cell clusters separated by sample. **c,** Violin plot of selected genes across different samples. **d,**
1240 Stacked bar plot showing the percentage of each cluster across different samples. **e,**
1241 Developmental pseudotime of T cells in a UMAP display. **f,** Cell trajectory analysis for T cells.

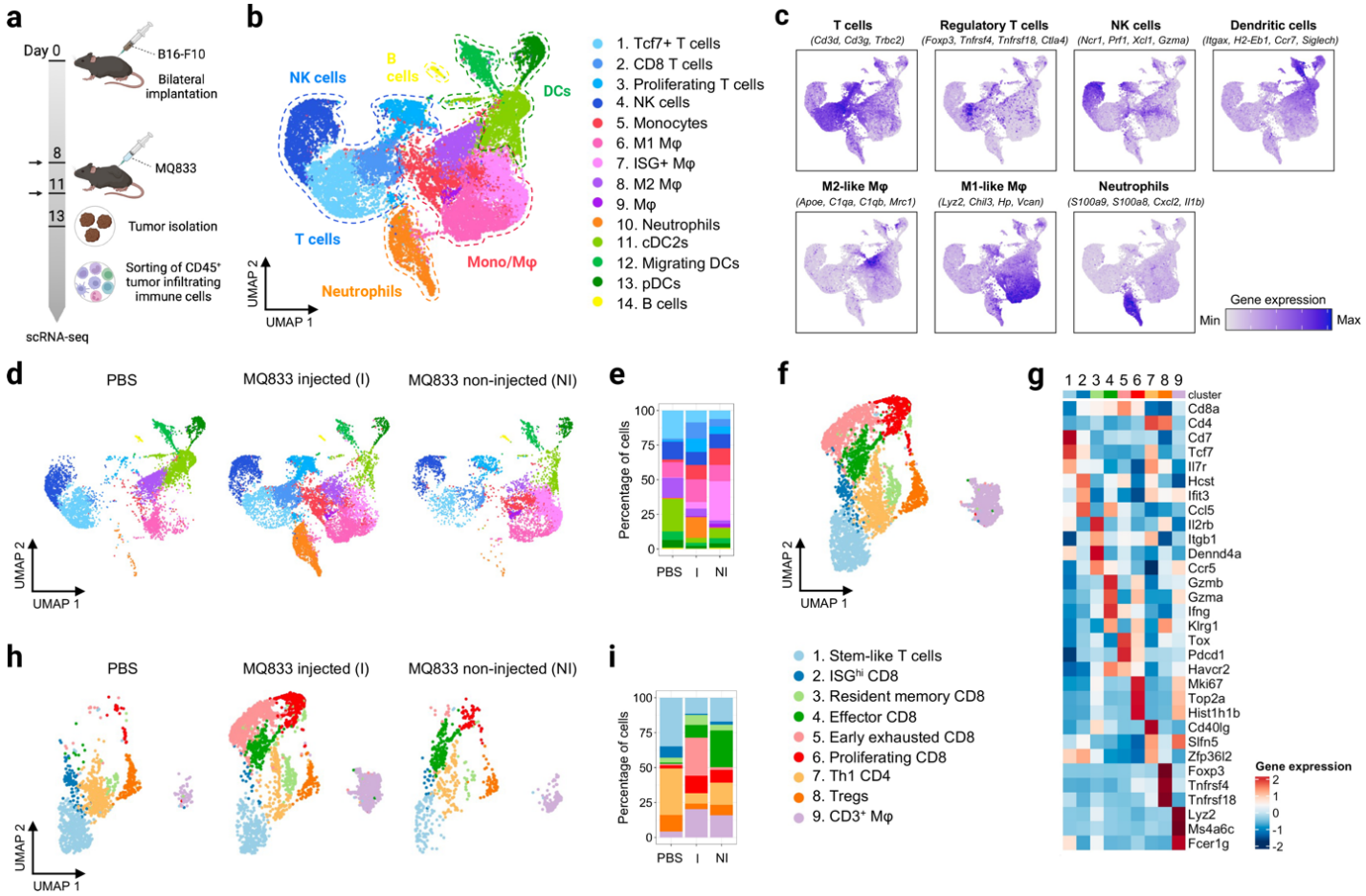
a
Day 0
B16-F10
Bilateral implantation
8
MQ833
11
13
Tumor isolation
Sorting of CD45+ tumor infiltrating immune cells
scRNA-seq
b
NK cells
B cells
DCs
T cells
Mono/Mφ
Neutrophils
UMAP 2
UMAP 1
1. Tcf7+ T cells
2. CD8 T cells
3. Proliferating T cells
4. NK cells
5. Monocytes
6. M1 Mφ
7. ISG+ Mφ
8. M2 Mφ
9. Mφ
10. Neutrophils
11. cDC2s
12. Migrating DCs
13. pDCs
14. B cells
c
T cells
(Cd3d, Cd3g, Trbc2)
Regulatory T cells
(Foxp3, Tnfrsf4, Tnfrsf18, Ctla4)
NK cells
(Ncr1, Prf1, Xcl1, Gzma)
Dendritic cells
(Itgax, H2-Eb1, Ccr7, Siglech)
M2-like Mφ
(Apoe, C1qa, C1qb, Mrc1)
M1-like Mφ
(Lyz2, Chil3, Hp, Vcan)
Neutrophils
(S100a9, S100a8, Cxcl2, Il1b)
Gene expression
Min
Max
d
PBS
MQ833 injected (I)
MQ833 non-injected (NI)
UMAP 2
UMAP 1
e
Percentage of cells
100
75
50
25
0
PBS
I
NI
f
UMAP 2
UMAP 1
g
1 2 3 4 5 6 7 8 9
cluster
Cd8a
Cd4
Cd7
Tcf7
Il7r
Hcst
Ifit3
Ccl5
Il2rb
Itgb1
Dennd4a
Ccr5
Gzmb
Gzma
Ifng
Klrg1
Tox
Pdcd1
Havcr2
Mki67
Top2a
Hist1h1b
Cd40lg
Slfn5
Zfp36l2
Foxp3
Tnfrsf4
Tnfrsf18
Lyz2
Ms4a6c
Fcer1g
Gene expression
2
1
0
-1
-2
h
PBS
MQ833 injected (I)
MQ833 non-injected (NI)
UMAP 2
UMAP 1
i
Percentage of cells
100
75
50
25
0
PBS
I
NI
1. Stem-like T cells
2. ISG^{hi} CD8
3. Resident memory CD8
4. Effector CD8
5. Early exhausted CD8
6. Proliferating CD8
7. Th1 CD4
8. Tregs
9. CD3^{+} Mφ

1242 **Fig. 5 | IT MQ833 reprograms TIME in both injected and non-injected tumors in a**
1243 **bilateral B16-F10 melanoma model. a**, Schematic diagram of the experimental schedule. B16-
1244 F10 cells were intradermally implanted into the right (5 x10^5) and left (2.5 x10^5) flanks of WT
1245 C57BL/6J mice. Once the tumors were established, two doses of IT MQ833 injection were given
1246 3 days apart. Tumors were collected 2 days after the second injection and processed into single
1247 cell suspension. CD45+ cells were sorted and sent for scRNA-seq. **b,** UMAP display of sorted
1248 CD45+ cells from 3 samples combined following 10X Genomics scRNA-seq workflow (n =
1249 21,675 cells). **c,** Expression plots of 7 main cell types using their top marker genes. **d,** UMAP
1250 plots of cell clusters separated by sample. **e,** Stacked bar plot showing the percentage of each
1251 cluster across different samples. **f,** UMAP display of subclustered $CD45^+CD3^+$ cells from 6
1252 samples combined following 10X Genomics scRNA-seq workflow (n = 4,901 cells). **g,** UMAP
1253 plots of cell clusters separated by sample. **h**, Stacked bar plot showing the percentage of each
1254 cluster across different samples. **i,** Heatmaps of the average expression of representative marker
1255 genes for each cluster.

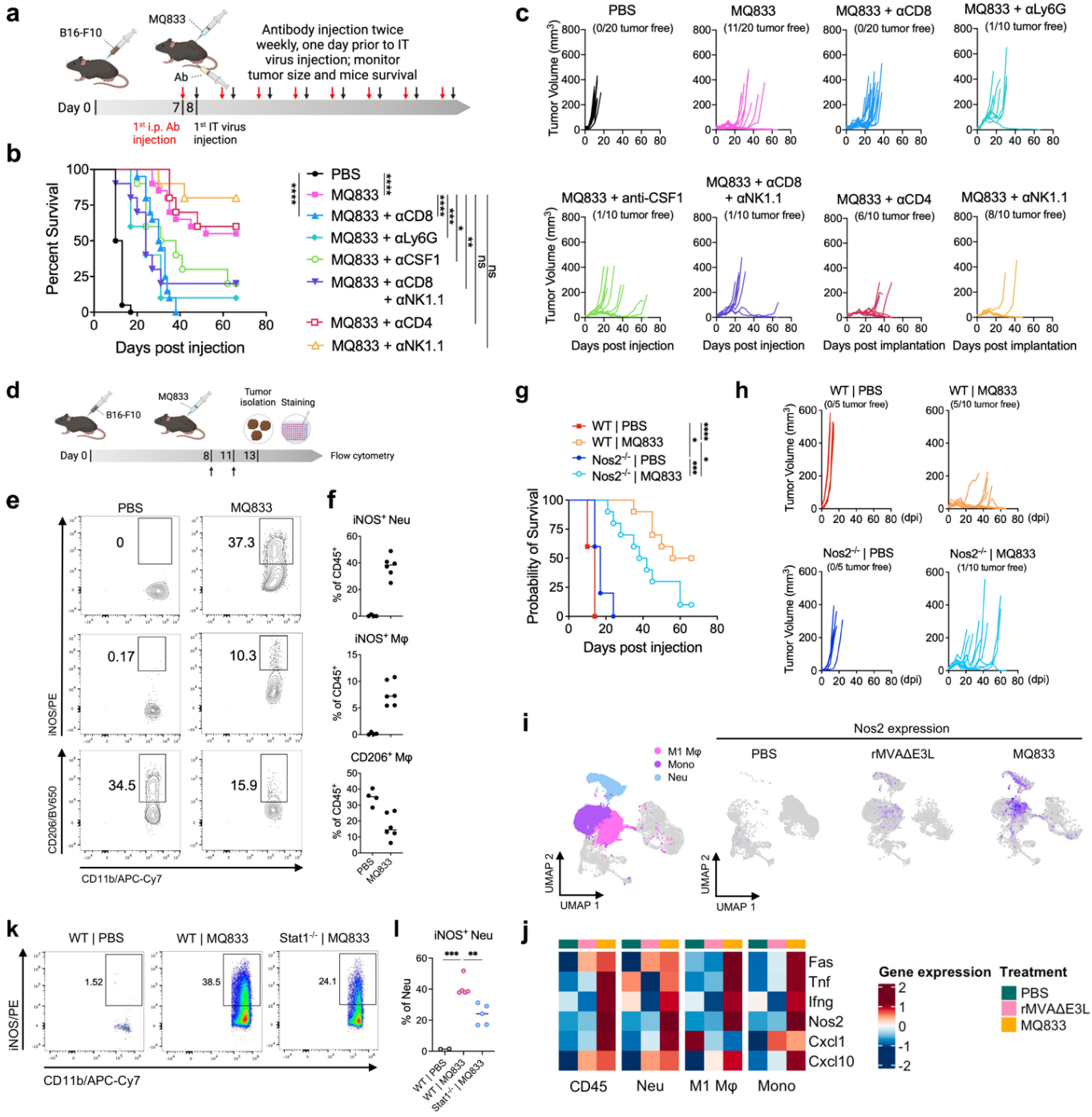
a
B16-F10
MQ833
Ab
Antibody injection twice weekly, one day prior to IT virus injection; monitor tumor size and mice survival
Day 0
7
8
1st i.p. Ab injection
1st IT virus injection
b
Percent Survival
Days post injection
PBS
MQ833
MQ833 + αCD8
MQ833 + αLy6G
MQ833 + αCSF1
MQ833 + αCD8 + αNK1.1
MQ833 + αCD4
MQ833 + αNK1.1
c
PBS (0/20 tumor free)
MQ833 (11/20 tumor free)
MQ833 + αCD8 (0/20 tumor free)
MQ833 + αLy6G (1/10 tumor free)
MQ833 + anti-CSF1 (1/10 tumor free)
MQ833 + αCD8 + αNK1.1 (1/10 tumor free)
MQ833 + αCD4 (6/10 tumor free)
MQ833 + αNK1.1 (8/10 tumor free)
Tumor Volume (mm3)
Days post injection
Days post implantation
d
B16-F10
MQ833
Tumor isolation
Staining
Day 0
8
11
13
Flow cytometry
e
PBS
MQ833
0
37.3
0.17
10.3
34.5
15.9
iNOS/PE
CD206/BV650
CD11b/APC-Cy7
f
iNOS+ Neu
iNOS+ Mφ
CD206+ Mφ
% of CD45+
PBS
MQ833
g
WT | PBS
WT | MQ833
Nos2-/- | PBS
Nos2-/- | MQ833
Probability of Survival
Days post injection
h
WT | PBS (0/5 tumor free)
WT | MQ833 (5/10 tumor free)
Nos2-/- | PBS (0/5 tumor free)
Nos2-/- | MQ833 (1/10 tumor free)
Tumor Volume (mm3)
(dpi)
i
Nos2 expression
M1 Mφ
Mono
Neu
PBS
rMVAΔE3L
MQ833
UMAP 1
UMAP 2
j
Fas
Tnf
Ifng
Nos2
Cxcl1
Cxcl10
CD45
Neu
M1 Mφ
Mono
Gene expression
Treatment
PBS
rMVAΔE3L
MQ833
k
WT | PBS
WT | MQ833
Stat1-/- | MQ833
1.52
38.5
24.1
iNOS/PE
CD11b/APC-Cy7
l
iNOS+ Neu
% of Neu
WT | PBS
WT | MQ833
Stat1-/- | MQ833

1256 **Fig. 6 | MQ33-induced antitumor immunity requires CD8$^+$ T cells, neutrophils, and**
1257 **macrophages, and *nos2* expression in myeloid cells plays a crucial role. a,** Schematic
1258 diagram of the experimental schedule. 5 x10^5 of B16-F10 cells were intradermally implanted into
1259 the right flanks of WT C57BL/6J mice. IT MQ833 injections were given twice a week once the
1260 tumors were established. I.p. αCD8, αCD4, αNK1.1, and αLy6G antibodies were given one day
1261 prior to every virus injection. I.p. αCSF1 were given every 5 days starting at one day prior to the
1262 first virus injection. Tumor size and mice survival were monitored. **b,** Kaplan-Meier survival
1263 curve of mice in each treatment group. PBS was used as a control. Survival data were analyzed
1264 by log-rank (Mantel-Cox) test (*n=10-20; *P < 0.05, **P < 0.01, ****P < 0.0001*). **c**, Tumor
1265 volumes of mice separated by group over days post treatment. (**d**,) Schematic diagram of the
1266 flow cytometry analysis experiment. **e**,**f**, Contour plots (**e**) and bar graphs (**f**) showing
1267 percentages of iNOS$^+$ cells among CD45$^+$CD3$^-$CD11b$^+$Ly6G$^+$ neutrophils (top row), CD45$^+$CD3$^-$
1268 CD68$^+$CD11b$^+$ macrophages (middle row), and percentages of CD206$^+$ cells among
1269 macrophages (bottom row) in MQ833 or PBS treated tumors. **g,h**, Survival study for B16-F10
1270 tumor-bearing mice treated with MQ833 in a *Nos2*$^{-/-}$ mouse model. 5x10^5 of B16-F10 cells were
1271 intradermally implanted into the right flank of *Nos2*$^{-/-}$ mice. IT MQ833 injections were given
1272 twice a week once the tumors were established. Tumor size and mice survival were monitored. **g**,
1273 Kaplan-Meier survival curve of mice in each treatment group. PBS was used as a control. (n=10)
1274 Survival data were analyzed by log-rank (Mantel-Cox) test (*n=5-10; *P < 0.05, ***P < 0.001,*
1275 *****P < 0.0001*). **h**, Tumor volumes of mice separated by group over days post treatment. **i,j**,
1276 scRNA-seq analysis of CD45$^+$ cells isolated from rMVAΔE3L or MQ833 treated tumors.. **i**,
1277 UMAP display showing *nos2* expression (right panel) in highlighted clusters (left panel) **j**, Heat
1278 maps showing average expression of selected antitumor marker genes in all the CD45$^+$ cells (first
1279 panel), neutrophil (second panel), M1-like macrophage (third panel), and monocyte (fourth
1280 panel) clusters divided by treatment groups.

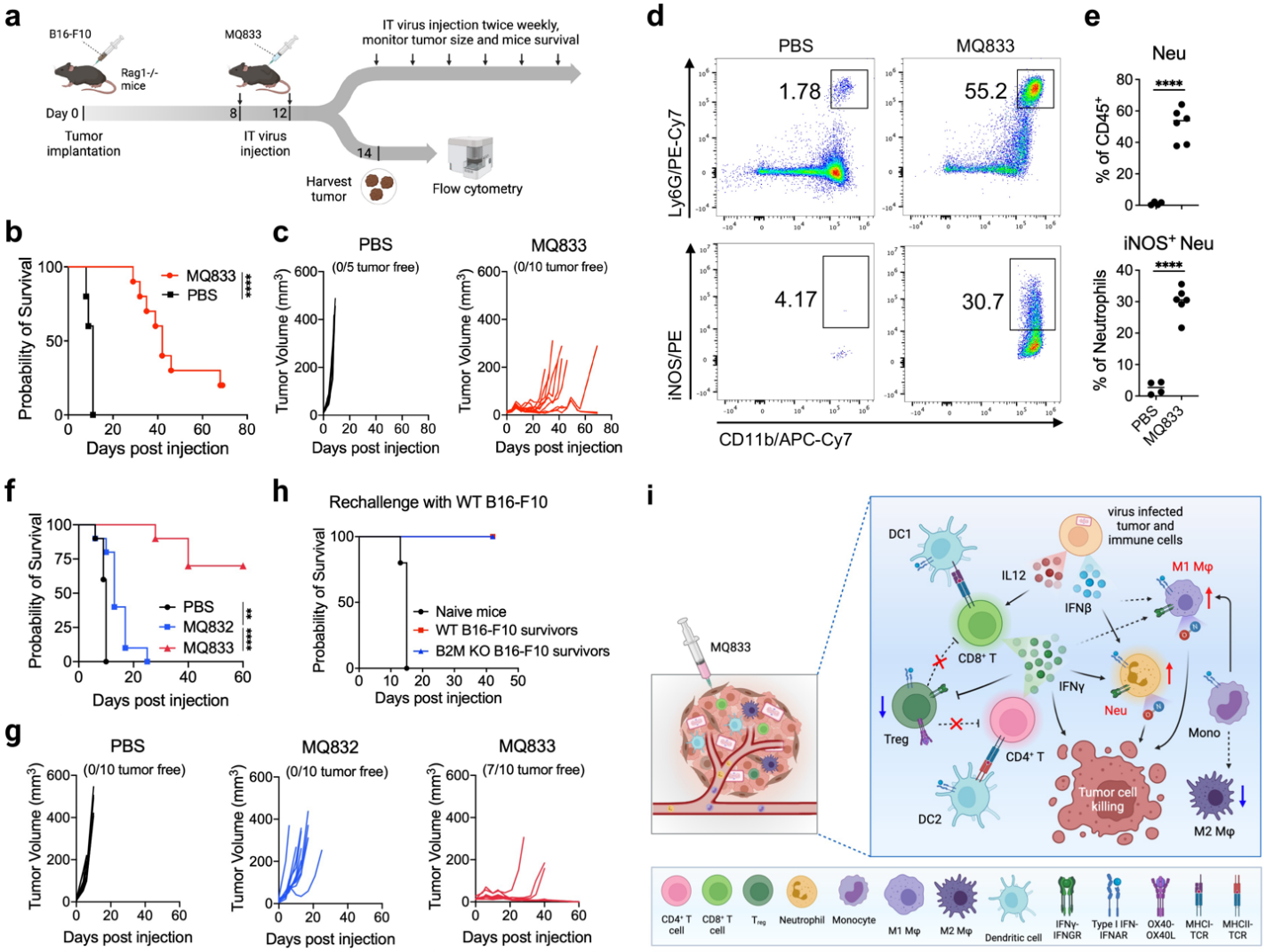
a
B16-F10
Rag1-/- mice
MQ833
IT virus injection twice weekly, monitor tumor size and mice survival
Day 0
8
12
14
Tumor implantation
IT virus injection
Harvest tumor
Flow cytometry
b
Probability of Survival
MQ833
PBS
****
Days post injection
c
PBS
(0/5 tumor free)
MQ833
(0/10 tumor free)
Tumor Volume (mm³)
Days post injection
d
PBS
MQ833
1.78
55.2
4.17
30.7
Ly6G/PE-Cy7
iNOS/PE
CD11b/APC-Cy7
e
Neu
% of CD45⁺
iNOS⁺ Neu
% of Neutrophils
PBS
MQ833
f
Probability of Survival
PBS
MQ832
MQ833
Days post injection
h
Rechallenge with WT B16-F10
Naive mice
WT B16-F10 survivors
B2M KO B16-F10 survivors
Days post injection
g
PBS
(0/10 tumor free)
MQ832
(0/10 tumor free)
MQ833
(7/10 tumor free)
Tumor Volume (mm³)
Days post injection
i
MQ833
DC1
virus infected tumor and immune cells
IL12
IFNβ
M1 Mφ
CD8⁺ T
IFNγ
Treg
Neu
Mono
CD4⁺ T
DC2
Tumor cell killing
M2 Mφ
CD4⁺ T cell
CD8⁺ T cell
Neutrophil
Monocyte
M1 Mφ
M2 Mφ
Dendritic cell
IFNγ-IFNGR
Type I IFN-IFNAR
OX40-OX40L
MHCI-TCR
MHCII-TCR

1281 **Fig. 7 | IT MQ833 treatment overcomes ICB resistance. a,** Schematic diagram of the survival
1282 and flow cytometry experimental design. 5 x10^5 of B16-F10 cells were intradermally implanted
1283 into the right flank of *Rag1*$^{-/-}$ mice. IT MQ833 injections were given twice weekly once the
1284 tumors were established. For survival study, tumor size and mice survival were monitored. For
1285 flow cytometric analysis, tumors were harvested at day 14 post implantation and tumor
1286 infiltrating immune cells were stained by fluorescent antibodies and analyzed by flow cytometry.
1287 **b,** Kaplan-Meier survival curve of mice in each treatment group. PBS was used as a control.
1288 Survival data were analyzed by log-rank (Mantel-Cox) test (*n=5-10; ****P < 0.0001*). **c**, Tumor
1289 volumes of mice separated by group over days post treatment. **d**,**e**, Dot plots (**d**) and bar graphs
1290 (**e**) showing percentage of $CD45^+CD3^-CD11b^+Ly6G^+$ neutrophils among total $CD45^+$ cells (top
1291 row) and $iNOS^+$ cells among neutrophils (bottom row) in MQ833 or PBS treated tumors. **f,g**, 1
1292 x10^6 of B2m$^{-/-}$ B16-F10 cells were intradermally implanted into the right flank of WT C57BL/6J
1293 mice. IT MQ833 injections were given twice weekly once the tumors were established. tumor
1294 sizes and mice survival were monitored. **f**, Kaplan-Meier survival curve of mice in each
1295 treatment group. PBS was used as a control. Survival data were analyzed by log-rank (Mantel-
1296 Cox) test (*n=10; **P < 0.01, ****P < 0.0001*). **g**, Tumor volumes of mice separated by group
1297 over days post treatment. **h**, Mice rejected primary B16-F10 or B2m$^{-/-}$ B16-F10 tumors were
1298 rechallenged with a lethal dose of B16-F10 tumor cells. Kaplan-Meier survival curve of the
1299 rechallenged mice. **i**, Working model illustrating the mechanisms of action MQ833.